RSC Advances

PAPER

View Article Online
View Journal | View Issue

Cite this: *RSC Adv.*, 2026, **16**, 17158

Structural studies, thermochromic luminescent properties and crystal-to-crystal transformation of a double-stranded Cu^{I}–I-bisquinoline coordination polymer

Cristian Pinzón-Vanegas,[a] Jorge J. Villa-Rivera,[a] Víctor Sánchez-Mendieta,[b] Diego Martínez-Otero,[b] Joaquín Barroso-Flores,[b] Alfredo R. Vilchis-Nestor,[b] Ginés Lifante-Pedrola,[c] Pilar Amo-Ochoa[de] and Alejandro Dorazco-González*[a]

The development of thermochromic luminescent materials with reversible chemical transformation capabilities based on earth-abundant metals is a central topic in materials chemistry. While several stimuli-responsive materials have been reported, compounds that respond to physical stimuli and can undergo single-crystal-to-single-crystal transformations (SCSC) are still rare. Herein, a new color-emitting Cu^{I} coordination polymer (CP), ^{1D}{[Cu$_2$(μ-I)$_2$(L)$_2$]·(CH$_3$CN)}, (L = synthetic ligand, *N*^{2},*N*^{6}-bis(quinolin-5-yl)pyridine-2,6-dicarboxamide), **CP1** was prepared, structurally described by single crystal X-ray diffraction at different temperatures and studied in detail as a multi-responsive luminescent material to temperature and mechanical force in the solid state. Upon excitation at 413 nm and low temperature of 97 K, **CP1** displays intense orange emission at 618 nm which is linearly quenched up to 191 K, subsequently, its emission is weakened under ambient conditions. The cuprophilic interactions ($d_{Cu-Cu=}$ 2.848 Å) formed at low temperature are particularly responsible for the intense color emission as evidenced by crystallographic studies and DFT calculations. Upon mechanical grinding of crystalline **CP1**, the amorphous material (**CP1**-G) presents a bright orange emission at 620 nm with a quantum yield of 0.51 and bi-exponential lifetime of τ_1 = 2.17 μs and τ_1 = 7.62 μs at ambient conditions. Based on multiple analytical tools (fluorescence, quantum yields, PXRD, IR-ATR, and lifetime) and SEM observations, this color emission is attributed to a desolvation process, involving CH$_3$CN molecules' release and formation of cuprophilic interactions. Mechanochromic luminescence and the crystalline phase of **CP1** can be reversibly restored by exposing the amorphous material to CH$_3$CN vapors. Furthermore, **CP1** exhibits a reversible SCSC transformation whereby the 1D-double-stranded stair polymer is converted into a 1D zigzag chain ^{1D}[CuI(L)], **CP2**, by controlled heating with drastic changes in the Cu^{I} coordination environment and in the crystal lattice. This work showcases the potential of Cu^{I}–I-bisquinoline-based materials for new applications.

Received 5th February 2026
Accepted 25th March 2026

DOI: 10.1039/d6ra01043a

rsc.li/rsc-advances

1 Introduction

The development of crystalline luminescent molecular compounds with external multi-stimuli response capabilities, through a quick change in their photophysical properties by modifications of physical or chemical environments, such as temperature, mechanical force or solvents, remains an active topic of research and an ongoing challenge in materials chemistry.[1–4] Among these multi-stimuli-responsive compounds, those that emit in the visible spectral region are highly desired in manifold fields of science and technology owing to a plethora of applications in sensing of chemical–physical parameters, actuation and optical storage devices.[5–7]

Fluorescent multi-stimuli compounds with mechano-, thermo- or solvatochromism have been dominated by synthetic organic crystals, arising from elastic π-conjugated structures derivative of carbazole,[6,8–10] cyanostyrene,[11,12] helicenes,[13] triphenylenes[14,15] benzofulvene,[16] and donor–acceptor fluorescent dyes.[2,17,18] Typically, these organic dyes exhibit intense color

[a]*Institute of Chemistry, National Autonomous University of Mexico, 04510, Mexico. E-mail: adg@unam.mx*
[b]*Centro Conjunto de Investigación en Química Sustentable, UAEM-UNAM (CCIQS), Carretera Toluca-Atlacomulco Km 14.5, C. P., Toluca, Estado de México 50200, Mexico*
[c]*Dpto. Física de Materiales, Universidad Autónoma de Madrid, Madrid, 28049, Spain*
[d]*Dpto. de Química Inorgánica. Universidad Autónoma de Madrid, Madrid, 28049, Spain*
[e]*Institute for Advanced Research in Chemical Sciences (IAdChem), Universidad Autónoma de Madrid, Madrid, 28049, Spain*

emission in the nanosecond range[8,9,18,19] and display efficient chromic responses to outer stimuli. However, they still suffer from some drawbacks such as too laborious synthesis, and short-live emissions, which may hamper their desired applications.[13] In the field of chromic stimuli-responsive materials, species which display long-lived emission in the microsecond range are of interest since their emission may be discriminated readily from scattered light and shorter lived background settings present in the real enviroments.[20–22] In this line, the literature features some heavy-metal-based complexes (Au^{I}, Pt^{II}, Ir^{III}) bearing P/N-donor ligands with phosphorescence dependent on temperature and mechanical stress.[23–27] Additionally, there are phosphorescent Ln^{III}-based complexes depicting a sub-group of external conditions responsive materials, such as thermal, magnetic, conductive, and mechanical parameters.[28–32] This class of precious and rare-earth metal compounds have predominated in the field of inorganic outer stimuli-responsive photochemical materials. However, their intended applications are seriously hindered due to their low commercial availability, high cost and toxic waste in the mining extraction.[33] In this context, molecular strategies for the creation of color emitting compounds with cheap, low-toxic and earth-abundant metals capable of modifying their emission by stimuli such as temperature or mechanical force, are of immerse importance for sustainable scientific applications.[34,35]

In recent decades, diamagnetic Cu^{I}–I-based compounds have emerged as a viable alternative for the development of chromatic luminescent materials, because they exhibit multiple color long-live photophysical mechanism[36] originated from excited triplet states derivative of metal-to-ligand charge transfers (^{3}MLCT) and d^{10}–d^{10} cluster-centered (^{3}CC) transitions (Cu^{I}, $3d^{10} \rightarrow 3d^{9}4s^{1}$).[37,38] The use of I^{-} anion favors the spin–orbit coupling (SOC), transitions between different multiplicities and the emission properties.[39] It is well-known that the color emission properties originated from cuprophilic interactions are strongly influenced by the molecular environment around the Cu^{I}-cluster, such as solvents, temperature and mechanical stress.[40–44]

Cu^{I}–I complexes bearing P/N/S-donor ligands (L) have drawn attention for their appealing structural diversity that include dimers $[Cu_2I_2L_n]$,[37,45–53] trimers $[Cu_3I_7L_n]$,[54] cubanes $[Cu_4I_mL_n]$,[36,42,50,55–59] hexamers $[Cu_6I_6L_n]$,[60] single chains $^{1D}[CuIL_m]_\infty$,[48,61] double chains $^{1D}[Cu_2I_2L_n]$[48,49,62–69] and layered networks $^{2D}[Cu_nI_nL_m]$.[50,70,71] Closed $Cu^{I}\cdots Cu^{I}$ interactions have contributed to achieve innovative structures striking emissive features.[43,72,73]

Cu^{I}–I complexes exhibit a wide set of geometries in the metal cluster due to the relatively small energy difference between the polymorphs where the final structure strongly depends on the synthetic conditions. In this line, the single-crystal-to-single-crystal transformation is an exciting topic and feasible property for these Cu^{I}–I materials; however, to date it has been little explored, compared to their optical or catalytical properties.[52,74] In general, understanding the photophysical and chemical mechanisms present in Cu^{I}–I-based chromatic materials that respond to multiple stimuli in the solid state remains a challenge.

Recent reports in nanochemistry have shown that $[Cu_2I_2$(-aminopyrazine)]-based on double-chain possess alterations of distances $Cu^{I}\cdots Cu^{I}$ depending on external mechanical stress.[3] So far, the overwhelming majority of staircase double-chain Cu^{I}–I compounds have been built with ligands containing only one ring of pyridine or pyrazine as revealed by recent reviews.[59,73,75]

Our interest in Cu^{I} coordination chemistry is mainly focused on self-assembly process with fluorescent bisquinoline ligands due to the scant research on their structures and their photophysical properties.

To our best knowledge, only one CP stair-case Cu^{I}–I with methylquinoline complex, which has green emission and d^{10} cuprophilic interactions.[76] Taking this into account, we surmised that a novel color emitting Cu^{I}–I CP with optical responses to physical stimuli and the ability to undergo single-crystal-to-single-crystal transformation (SCSC) can be created using a ditopic bisquinoline ligand that in principle can amplify the possibility of metallophilic interactions.[77]

The results obtained for a novel double-stranded staircase Cu^{I}–I CP including synthesis, X-ray single crystal structural studies at different temperatures, its orange-emitting evolution under thermal and mechanical stimuli in solid state, as well as a SCSC transformation and theoretical DFT studies are summarized below.

2 Results and discussion

2.1 Crystal structure, characterization and morphology of $^{1D}[Cu_2(\mu\text{-}I)_2(L)_2]_\infty$, CP1

Cu^{I}–I-based compounds appending a quinoline ring as ligand have shown rich photoluminescence properties with yellow/orange emissions (~590–650 nm)[76,78,79] and these have been used as amino acid sensors, and mechanochromic materials. However, reversible luminescent response to multiple stimuli at the molecular level and crystal-to-crystal transformations remain largely unexplored.

For these investigations, a new Cu^{I}–I-bisquinoline compound, **CP1**, was synthesized by a solvothermal method through the reaction of CuI with N^2,N^6-bis(quinolin-5-yl) pyridine-2,6-dicarboxamide (L) in CH_3CN using equimolar amounts (Scheme 1).

L was synthesized by a modification of a previously reported method[80,81] and it was pure according to ^{1}H, ^{13}C, MS-DART(+) analysis (Fig. S1–S3). Single crystal X-ray diffraction of Cu^{I}–I-bisquinoline at different temperatures (100, 150 and 293 K, Table S1, SI) reveals that **CP1** crystallizes in the monoclinic *C*2/*c* space group with formula $^{1D}\{[Cu_2(\mu\text{-}I)_2(L)_2]\cdot(CH_3CN)_{0.88}\}_\infty$. **CP1** is constructed from a double staircase chain with asymmetric rhombohedral $[Cu_2(\mu\text{-}I)_2]$ dimers and coordinated to ligands (L) at periphery of staircase (Fig. 1A and S4). Such structure is still rare, and there are only a few examples, such as, $[Cu_2I_2(Py)]$,[49,62,65–67] $[Cu_2I_2$(pyrimidines)][63] and $[Cu_2I_2$(pyrazine)].[48,68,69]

It is noteworthy that **CP1** represents the first example of a double staircase structure bearing a bisquinoline ligand (Fig. 1B) where the asymmetric unit involves half of $[Cu_2(\mu\text{-}I)_2]$

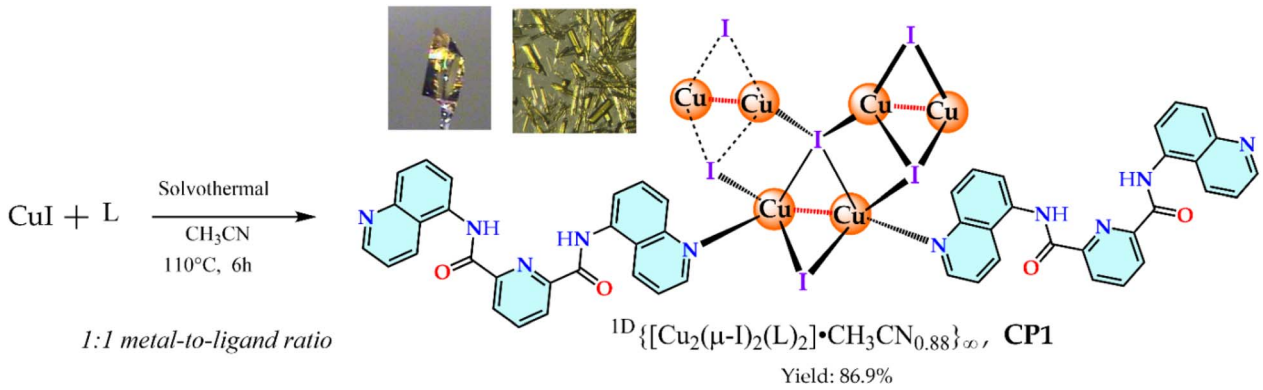

Scheme 1 Synthetic path for **CP1**. Inset: photographs of single crystals under natural light.

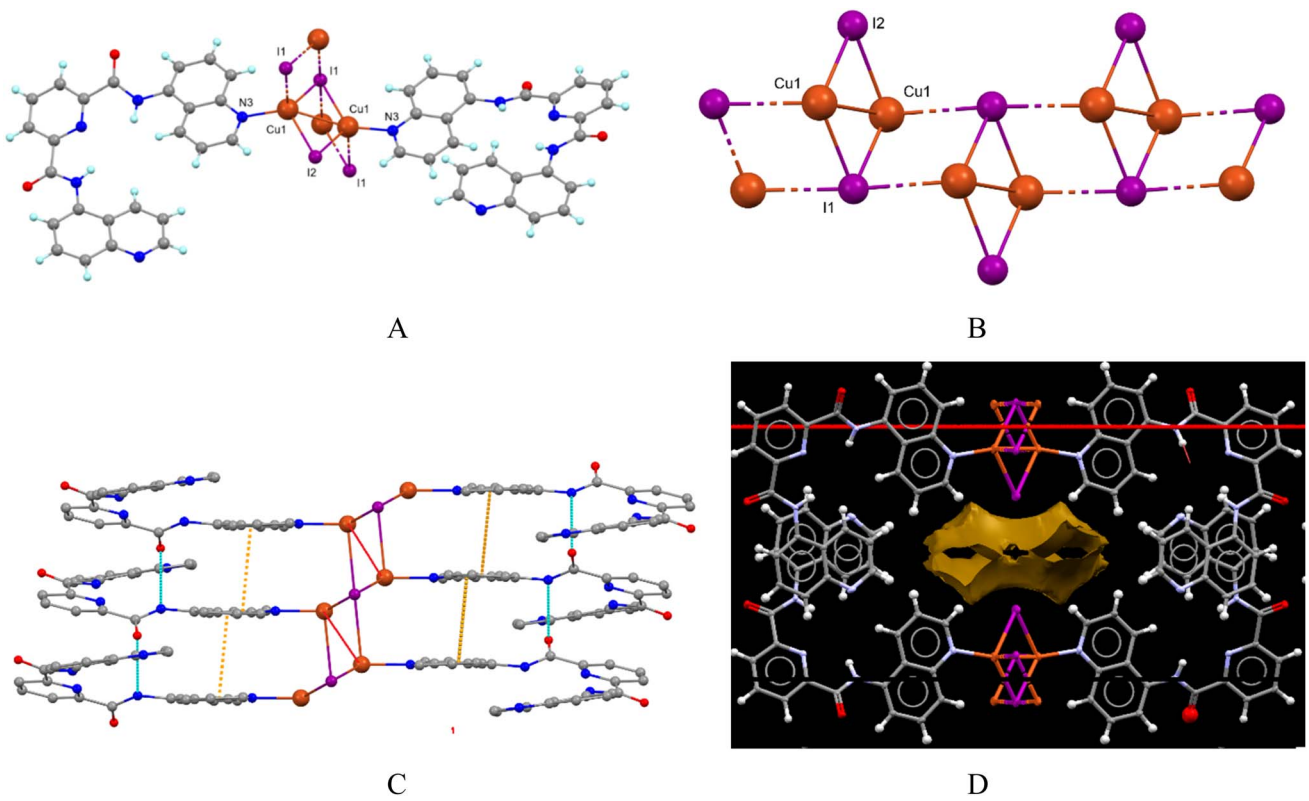

Fig. 1 (A) Perspective view of crystal structure of **CP1** in a ball and stick model. (B) 1D double-strained staircase chain formed by $[Cu_2(\mu\text{-}I)_2]$ cluster along *c* axis. (C) intermolecular H-bonds (N–H···O, cyan dashed lines) between amide groups and π···π stacking interactions (3.731(4)–3.736(6) Å orange dashed lines) measured between the quinoline rings. Hydrogen atoms and solvent molecules are omitted for clarity. (D) Depiction of void surfaces (gold) for a packing section of **CP1** along *c* axis. Atom codes: Cu (orange), I (purple), C (grey), O (red), N (blue) and H (white).

cluster and one L unit. Each Cu^I atom is coordinated by three I^- anions and one quinoline ring forming a distorted tetrahedral geometry of $[CuI_3N]$ type (see Table S2 for selected distances and angles around the Cu^I atom). The Cu^I–I cluster includes two crystallographically independent I^- atoms which bridge the metal centers in μ_4-I(1) and μ_2-I(2) coordination modes.

The Cu^I–I bond distances ranging from 2.5870(4) Å to 2.9025(5) Å and Cu^I–N bond distance is 2.037(2) Å at 100 K. All of them are within the range of values found in Cambridge Structural Database (Cu^1–I ~2.66(5) Å and Cu^I–N ~2.04(3)Å).[43,76] The shorter $Cu^I\cdots Cu^I$ distance (2.849(3) Å) is close to the sum of van der Waals radii of Cu^I atoms (2.85 Å)[69] suggesting a cuprophilic interaction, which is favorable to our aims because this interaction is the cause of the emission in several compounds. The hydrophobic bisquinoline ligands wrap around the double-stranded Cu^I–I chain *via* a Cu–N coordination bonds with one of the quinoline unit; interestingly, the second quinoline unit remains uncoordinated. The ligands are tightly packed by

intermolecular H-bonds between the amide groups (N–H···O=C, see Table S3 for H-bonding parameters within crystal packing) and multiple stacking π···π interactions (ranging from 3.731(4) Å and 3.736(6) Å) between quinoline rings as shown in Fig. 1C and S5. Eventually, each one double-stranded Cu^{I}–I chain has the shape of half a square prism which is linked to another chain by π···π interactions of the uncoordinated quinoline arm closing a complete square prism-shape structure as is depicted in Fig. 1D.

PLATON software calculations[82] yield a solvent accessible volume of 6.66% of the total volume, corresponding to 314.7 A^3 out of 4734.4(3) $Å^3$ per unit cell volume available in the crystalline structure of **CP1**. These small channel-shaped voids (dimensions ~7.5 Å × 13.8 Å) are occupied by crystallization CH_3CN molecules as depicted in Fig. 1D, S6 and S7. IR-ATR spectrum of crystalline sample of **CP1** (Fig. S8) shows a low-intensity band (cm^{-1}) characteristic for CH_3CN at 2254 (C≡N stretching).[83] The low band intensity may be a result of the occupational (0.88) and positional disorders of this molecule inside the voids. The intermolecular H-bonds between the amide groups observed in the crystal structure are evidenced in IR-ATR spectra when compared the bands of **CP1** with the free ligand ($\Delta\nu_{(N-H)}$ = 139 cm^{-1}). Elemental analysis (C, H, N) matched perfectly to crystal structure. A comparison of the powder X-ray diffraction (PXRD) pattern of a bulk sample of freshly synthesized **CP1** with the simulated pattern of the crystal structure matches well with respect to the main peaks and intensities (Fig. 2A), confirming the high purity of the phase. Thus, this crystalline sample was used for further multi-stimuli experiments and crystal-to-crystal transformation.

The morphology and elemental distribution of crystals of **CP1** were examined by Scanning Electron Microscopy (SEM) equipped with an Energy Dispersive X-ray (EDS) detector.

SEM analysis revealed that this Cu^{I}–I-based material exhibits a smooth surface and large block-like morphology at the micrometer level (Fig. 2B), their growth seems layer-by-layer, as shown in Fig. S9. Moreover, the elemental distribution observed in the EDS mapping (inset Fig. 2B) indicates a homogeneous distribution of all elements throughout the single crystal. The carbon content obtained from EDS measurements (49.69%) closely agrees with the value determined from elemental analysis (C = 49.75%), further confirming the composition and purity of **CP1**. The thermal analysis (TGA) of **CP1** from 25 °C to 700 °C (Fig. S10) under N_2 atmosphere shows thermostability up to 220 °C. After that, a three-steps mass breakdown process was observed. The first weight breakdown loss (65.83%), between 240 °C and 430 °C, corresponds to the loss of L (calcd, 66.07%), while the second weight loss (19.51%) through 450 °C to 580 °C, corresponds to the loss of I atoms (calcd: 20.80%). Finally, the remaining mass (14.66%) coincides with that estimated for CuO (calcd 13.04%).

2.2 Temperature single crystal X-ray diffraction and thermochromism of CP1

Firstly, single crystal X-ray data for **CP1** were collected at three different temperatures to gain further insight the correlation between intended luminescent thermochromism and $Cu^{I}\cdots Cu^{I}$ distances, as well as to detect the potential change in molecular structure of $^{1D}[Cu_2(\mu\text{-}I)_2]$ cluster. Temperature-dependent X-ray crystallographic data at 100 K, 150 K and 293 K (Table S1) shows that cell volumes of the single crystal get considerable smaller (~146 $Å^3$, *ca.* 3%, Table 1) as the temperature decreases. It is reasonable to assume that the contraction of the unit cell shortens the distance between Cu^{I} atoms and the bond distances of the I^-/N atoms of the ligands in the core. Upon cooling at 100 K, the $Cu^{I}\cdots Cu^{I}$ distances are substantially shorter (~4.2%) compared to those found at 293 K, from 2.970(3) Å to 2.8482(8) Å as shown in Fig. 3 and Table 1.

Conversely, distances I(1)···I(2) enlarged from 4.309(4) Å to 4.385(5) Å because of the rhombohedral Cu^{I}–I(1)–Cu^{I}–I(2) core contraction. On the other hand, the angles Cu^{I}–I–Cu^{I} and

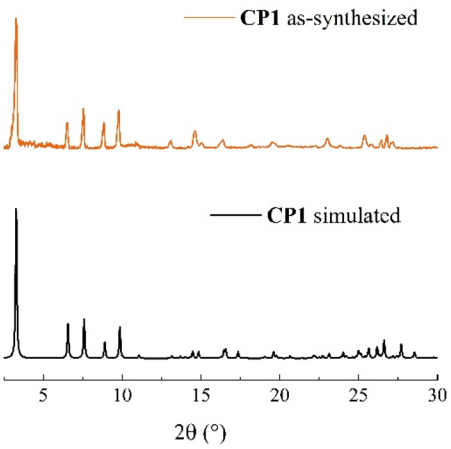

A

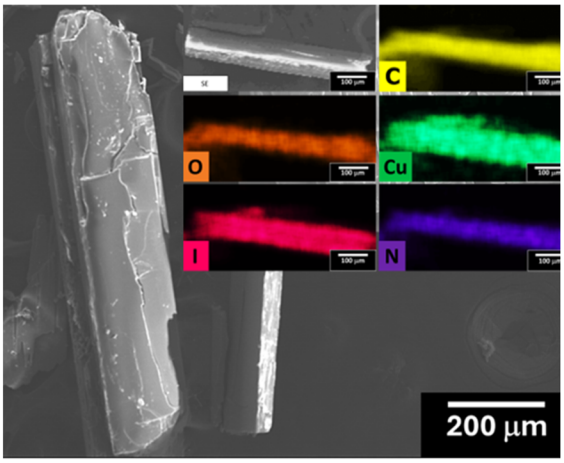

B

Fig. 2 (A) Experimental and simulated PXRD (Cu K_α) pattern of **CP1**. (B) SEM images of the as-synthesized **CP1**. Inset: EDS chemical mapping elements showing O, I, C, Cu and N signals.

Table 1 The Cu^{I}–I/Cu–N bond distances, $Cu^{I}\cdots Cu^{I}$ interactions (Å) and cell volume (Å^3) of the single crystal of **CP1** at three different temperatures

	100 K	150 K	293 K
I(1)–Cu(1)	2.5870(4)	2.5812(12)	2.5823(14)
I(2)–Cu(1)	2.6424(5)	2.6478(14)	2.6515(16)
I(1)–Cu(1)#2	2.9025(5)	2.8988(14)	2.9079(19)
Cu(1)–N(3)	2.037(2)	2.034(6)	2.042(16)
Cu(1)–Cu(1)	2.8482(8)	2.885(2)	2.970(3)
I(1)–I(2)	4.385(5)	4.361(3)	4.309(4)
Cell volume	4734.4(3)	4774.7(6)	4880.46(12)

I(1)–Cu^{I}–I(2) are reduced (68.13° → 65.24°) and increased (110.83° → 113.98°), respectively.

Instead, Cu^{I}–N and Cu^{I}#2-I (adjacent $[Cu_2I_2]$ units) bond lengths remain practically constant. Interestingly, at all temperatures the atoms that form the rhombohedral Cu^{I}–I(1)–Cu^{I}–I(2) cluster are perfectly coplanar. Despite the known correlation between bond distances in Cu^{I}–I-based compounds and their emission properties at different temperatures, very few studies have reported Cu^{I}–I and $Cu^{I}\cdots Cu^{I}$ bonding trends from experimental X-ray diffraction data at different temperatures[43,74,84] which is crucial for better understanding of thermochromism and other cuprophilic interactions-dependent phenomena.

From the comparison of these temperature-dependent structural findings, it is possible to predict that **CP1** will display greater color emitting properties at low temperature. At room temperature, **CP1** is a bright yellow solid with a weak orange emission under UV light (see Scheme 1). However, a bright orange emission appears after **CP1** manual grinding (~10 min) or when cooling this compound at N_2 liquid temperature, this behavior is displayed in Fig. 4. These photophysical phenomena are reversible. **CP1** loses its intense color emission significantly when warmed up to room temperature or several hours after it was ground.

CP1 solid-state UV-vis absorption spectrum under ambient conditions shows a broad/intense band in the range from 290 nm to 420 nm and a very weak band at 495 nm (Fig. S11).

Upon excitation at 413 nm and at 100 K, the powder sample of **CP1** exhibits an intense emission band centred at 612 nm, which is consistent with the observed orange emission (Fig. 5A, watch Video1 SI).

Simultaneously, a higher-energy band around 470 nm is observed, which is commonly found in quinoline moieties, ascribed to intraligand (IL) electronic transitions involving π* orbitals of the unsaturated rings.[77]

The free ligand L displays only a single high energy blue emission band centred at 450 nm upon excitation at 360 nm in the solid state, which is attributed to intraligand n–π*and π–π*charge transfer.[43,77]

By comparing the emission spectra of L and **CP1**, it is reasonable to think that low energy color emission at 620 nm originates from the Cu^{I}–I cluster and metal–ligand contributions.

The corresponding excitation spectrum (λ_{em} = 610 nm) of **CP1** at 100 K displays a broad and high-energy band ranging from 290 to 415 nm with a maximum at 360 nm. At 100 K, the emission intensity of **CP1** at 612 nm shows ~8-fold increase in intensity compared to its room temperature spectrum (Fig. S12). This improvement in intensity is sufficient for the orange emission to be observed with the naked eye. Similar orange emission bands within range from 570 nm to 630 nm have been reported by some Cu^{I}–I CPs/dimers with S-/N-donor ligands, and these are typically assigned to a combination of MLCT and a metal cluster centered [^{3}MCC, d_{Cu} → $(s,p)_{Cu}$] transitions.[3,67,74,76,84–88] The involvement of cuprophilic interactions in the deep orange emission of **CP1** at low temperature is unambiguously supported by crystallographic studies at 100 K (*vide supra*).

Next, temperature-dependent emission spectra (λ_{ex} = 413 nm) of **CP1** were recorded between 97 K and 221 K to track its thermochromism (Fig. 5B).

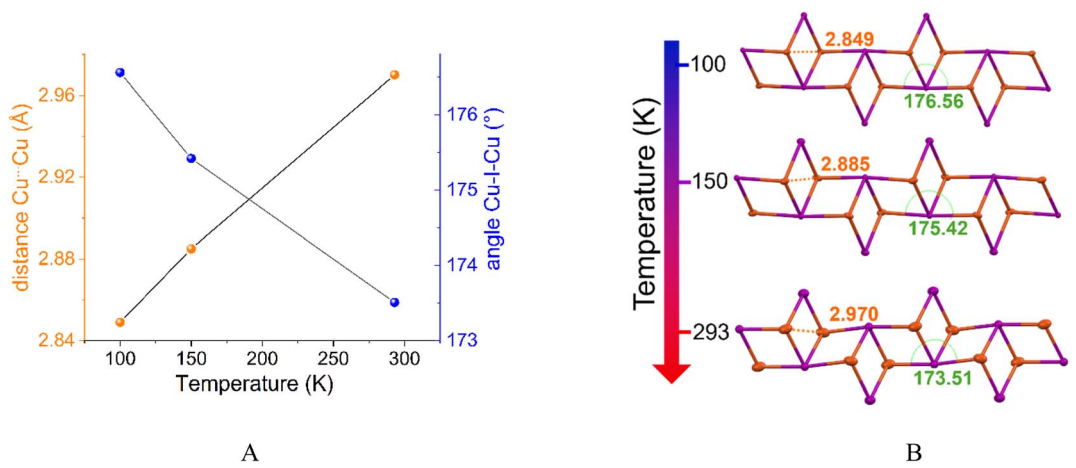

Fig. 3 (A) $Cu^{I}\cdots Cu^{I}$ distances and Cu–I–Cu angles from X-ray crystal structures of **CP1** at three different temperatures. (B) molecular structures of the Cu^{I}–I **CP1** at 293 K, 150 K and 100 K showing $Cu^{I}\cdots Cu^{I}$ distance.

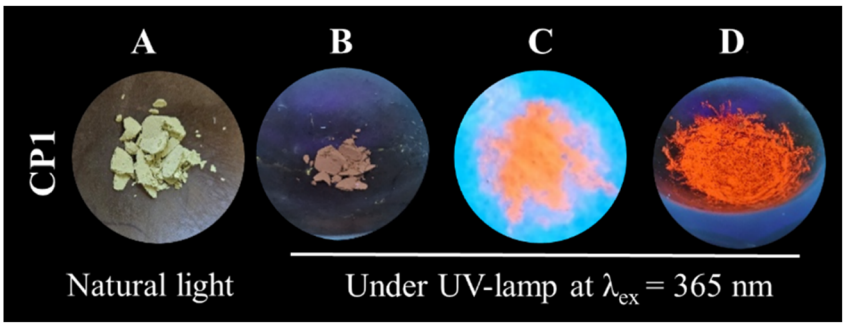

Fig. 4 (A and B) Photos of **CP1** at 293 K under natural light and UV irradiation. (C) at low temperature and (D) after grinding under UV light.

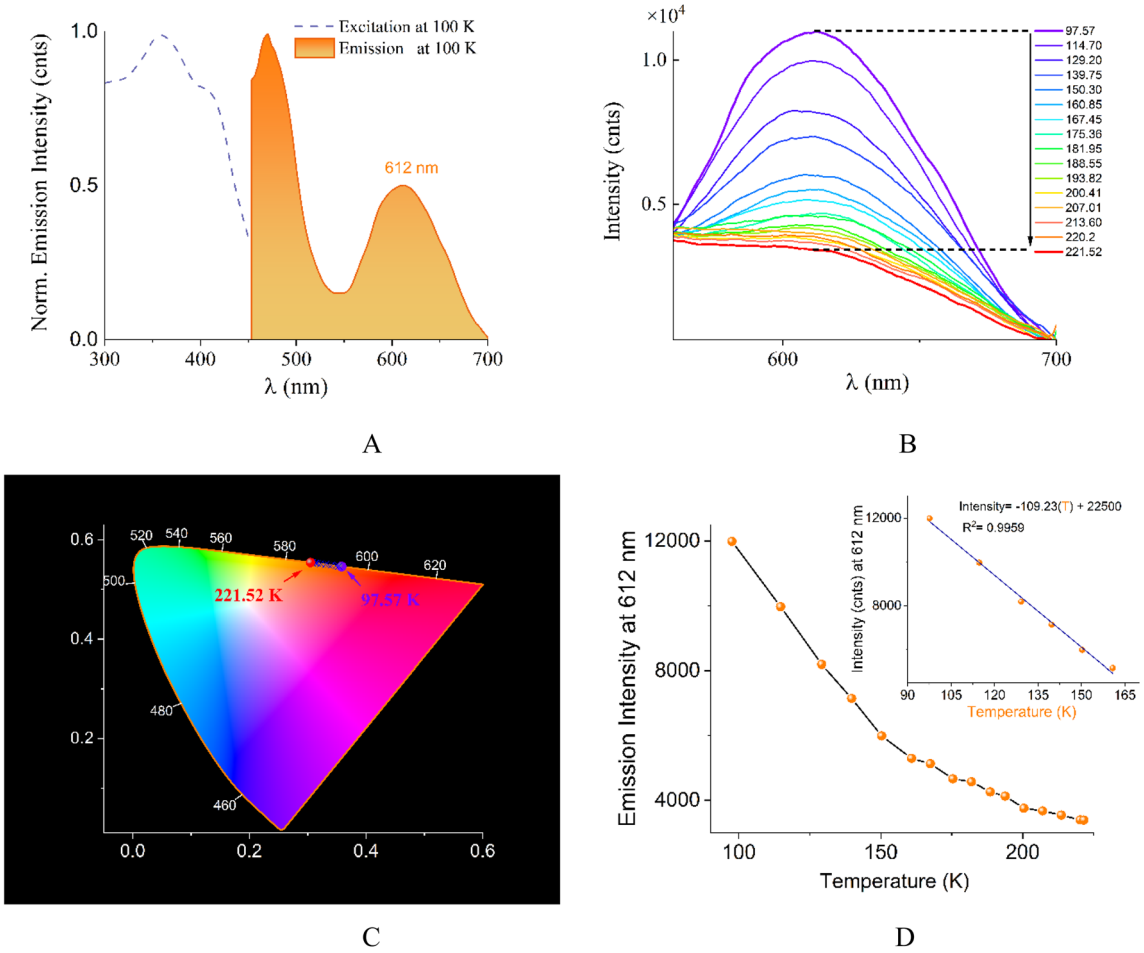

Fig. 5 A) Luminescence excitation (λ_{em} = 610 nm) and emission (λ_{ex} = 413 nm) spectra of **CP1** at 100 K. (B) Fragment in the visible range of emission spectra of **CP1** at different temperatures (K). (C) CIE-1931 and (D) intensity at 612 nm at variable temperature. Inset: solid line was obtained by linear fitting.

At 221 K, the luminescence spectrum displays an unstructured broad emission band. Conversely, lowering the temperature to 97 K results in a significant increase in intensity with the formation of a well-structured band centred at 612 nm. Additionally, a modest shift (9 nm) towards red of the band maximum was observed from 603 nm (CIE coordinate, $X = 0.30$, $y = 0.55$) to 612 nm (CIE, $X = 0.36$, $y = 0.54$), as illustrated in chromaticity diagram (Fig. 5C). It is well documented that a decrease of $Cu^{I}\cdots Cu^{I}$ distances are responsible for red shifting in a low energy bands (visible region),[89] particularly at low temperature, while the increase of the Cu⋯Cu distance[90] and/or contribution from MLCT/LMCT is associated with blue-shift both in low energy and higher-energy bands closest to UV region.[76,90–92] Previous theoretical works have demonstrated that attractive cuprophilic interactions within Cu^{I}–I complexes in the excited state (LUMO) are of bonding character.[93] Thus, when

the temperature decreases result in (1) $Cu^{I}\cdots Cu^{I}$ shorter distances, (2) an increase in the binding character and (3) energy levels drop.[60,93]

Thus, the energy difference between excited states and the ground state becomes smaller. Hence, low-energy emission bands correspond to transition from excited states of shorter $Cu^{I}\cdots Cu^{I}$ bonds.[34,74,89]

The emission intensity at 612 nm drastically increases as the temperature decreases as a result of the formation of cuprophilic interactions at low temperature (see Table 1).

Fig. 5D shows the thermal quenching effect of **CP1** at 612 nm. Notably, there was a linear dependence of the luminescence intensity on the temperature in the range of 97–191 K. This linear data can be well fitted to eq. Intensity = 22 500–109.23[T], with a correlation coefficient ($R^2 = 0.9959$). Above 200 K the emission intensity is very weak, and it remains practically constant. From structural X-ray analyses, it is observed that the Cu–N and Cu^{I}–I distances practically do not change at different temperatures; therefore, the increase in emission can be attributed mainly to the shortening of the cuprophilic distances.

2.3 Mechanochromism by grinding

The first evidence of mechanochromic luminescence of **CP1** was obtained by manual grinding (10 min) at room temperature using a pestle (ground sample named **CP1**-G). Upon grinding, a naked eye intense orange emission luminescence is generated under UV light at 365 nm (Fig. 4). On the other hand, no color changes were detected in the sample under natural light.

After treatment of **CP1**-G with CH_3CN fuming (10 min), the orange emission is turned off almost completely returning to its initial naked eye non-emissive state. This turn-on and off emission change of **CP1** was observed in repeating cycles of grinding and treating the sample with CH_3CN vapors. Fig. 6A shows the emission spectra ($\lambda_{ex} = 425$ nm) of starting unground sample of **CP1**, and ground sample **CP1**-G at ambient temperature. Clearly, the color emission intensity centred at 612 nm turns on after grinding. The absolute quantum yield (Φ) of emissive compound **CP1**-G is 0.51 and upon excitation with a 405 nm laser at ambient temperature, its emission decay shows a bi-exponential lifetime (τ = 2.17 μs and 7.62 μs), monitored at 645 nm (Fig. 6B). The μs scale for these long-live

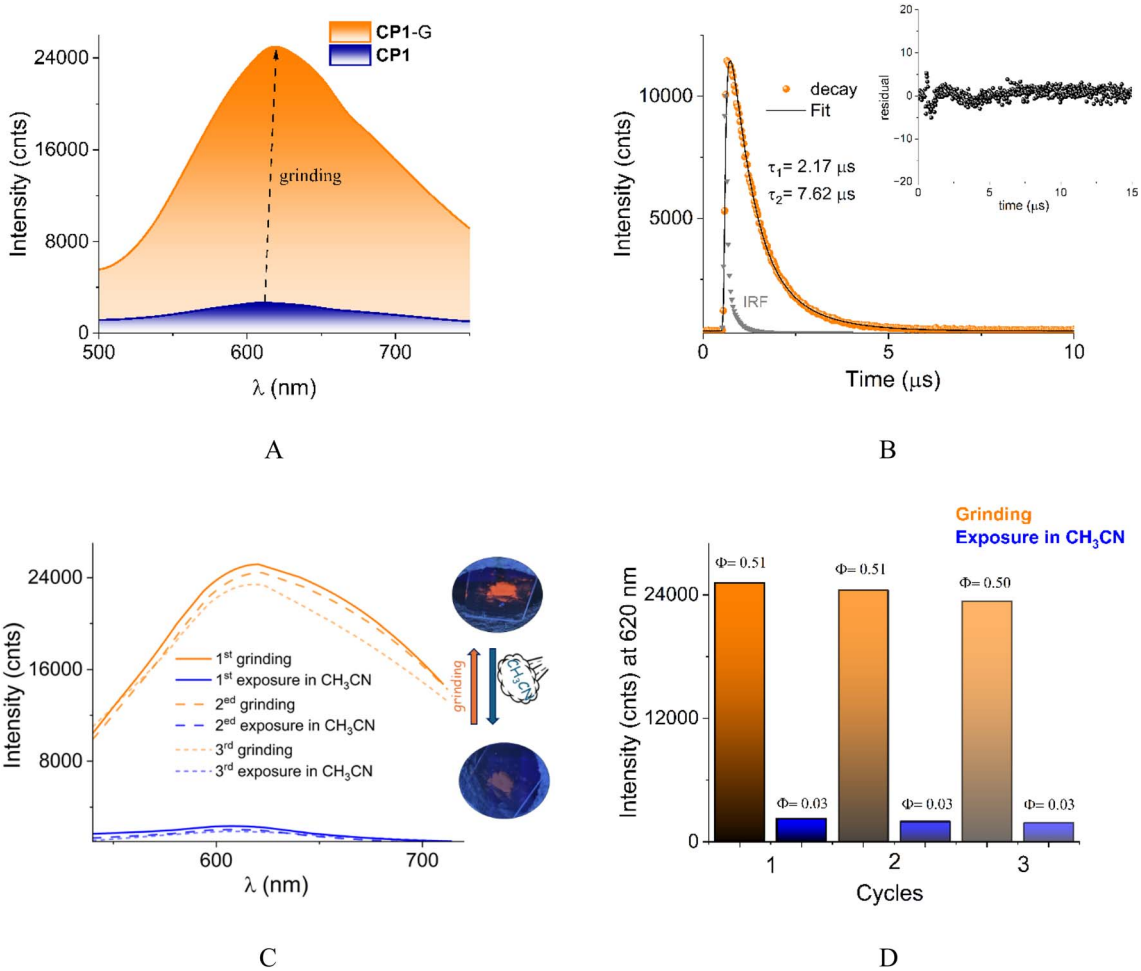

Fig. 6 (A) Emission spectra ($\lambda_{ex} = 425$ nm) of **CP1** and **CP1**-G at room temperature. (B) Luminescence decay at room temperature of **CP1**-G upon excitation 405 nm laser and monitored at 645 nm. The solid line was obtained by a bi-exponential fitting with a goodness-of-fit parameter $\chi^2 = 0.994$. The IRF is shown in grey. Inset: residual plot. (C) emission spectra ($\lambda_{ex} = 425$ nm) of **CP1** and (D) emission intensities at 620 nm and Φ in the different states of the cycles of grinding (10 min) and exposure to CH_3CN vapor (10 min).

emissions are common for Cu^{I}-halide-based clusters involving triplet states ^{3}CC which implies presence of cuprophilic interactions.[2,3,67,71,94–97] Indeed, ^{3}CC emissions are dependent on the Cu^{I} cluster cores and are independent of the coordinated ligands.[43] Therefore, this lifetime in μs range strongly suggests the presence of cuprophilic interactions induced in **CP1**-G.

Conversely, **CP1** before grinding shows a very low emission intensity in the visible region with a Φ of 0.03, which is consistent with the virtually zero color emission of this sample under the UV lamp. The luminescence decay of **CP1** (before the grinding process) monitored at low energy, particularly in the color emission region at 645 nm (λ_{ex} = 405 nm) is almost zero. The absence of color emission indicates that unground **CP1** in its crystalline state at room temperature does not present cuprophilic interactions, as proved in its crystallographic studies at 293 K.

To insight the mechanism of the reversible mechanochromic luminescence of **CP1**, unground, ground and recovered samples with CH_3CN of three cycles were analyzed by fluorescence spectroscopy, quantum yields, IR-ATR, PXRD and SEM. To avoid misunderstanding, we have named the treated samples with CH_3CN as **CP1**-R.

Fig. 6C shows the emission spectra of **CP1** in different states of grinding/treatment with CH_3CN. In all cycles, the ground samples (**CP1**-G) show the intense emission band centred at 612 nm together with Φ values around ~0.5, which is consistent with the intense solid-state orange luminescence visually perceived under UV light (Fig. 6D).

On the other hand, treated samples with CH_3CN fuming (**CP1**-R) display a very low intense emission band centred at 610 nm with Φ values <0.03. This low intense emission band in the **CP1**-R samples is almost the same as that observed in the spectrum of crystalline **CP1** before grinding.

IR-ATR spectra of **CP1** during the cycles (Fig. S13) practically do not show changes in the main ligand bands ($\nu_{(C=N)}$ = 1524 cm^{-1}, $\nu_{(C=O)}$ = 1688 cm^{-1} and, $\nu_{(N-H)}$ = 3324 cm^{-1}). This suggests that there are no chemical modifications regarding the modes of coordination of the ligand with the Cu^{I} atoms.[40] After treating the samples with the solvent (**CP1**-R), a weak band is observed at ~2255 cm^{-1}, which can be assigned to the presence of CH_3CN in the **CP1** void spaces, as observed in its crystalline structure (Fig. S6).

Elemental analysis (C, H, N) of unground crystalline sample **CP1** and amorphous **CP1**-G gave the expected composition (Table S4) for solvated and non-solvated samples, respectively, which supports the removal of solvent CH_3CN molecules by the grinding process.

To confirm that the original structural arrangement of **CP1** is maintained during mechanochromism by grinding and subsequent treatment with CH_3CN, PXRD experiments were caried out in the different states of the cycles (Fig. 7). Initially, the grinding practically eliminates the diffraction peaks (**CP1**-G), which suggests a very strong reduction in the crystalline domains.[43,89,92] Upon treating of ground sample **CP1**-G with CH_3CN vapors, the original diffraction peaks at 6.53, 7.51, 8.86, 9.75, 14.62, 16.43 and 28.81° corresponding to crystalline structure (**CP1**) are restored, and no new peaks appear.

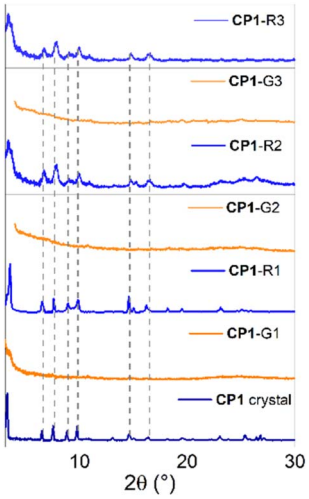

Fig. 7 PXRD (CuK_α) patterns of unground crystalline sample (**CP1**), ground samples (**CP1**-G) and treated samples with CH_3CN (**CP1**-R) for different states of the cycles. The dashed gray lines indicate the main diffraction peaks.

However, the recovered **CP1**-R recovered PXRD peaks are broader and present some differences in the reflection intensity, which is probably due to (1) a partial reconstitution of the crystalline phase and (2) an orientation effect in powders as described for some Cu^{I}–I complexes treated by grinding and solvation processes.[43,98]

SEM observations of **CP1**, **CP1**-G and **CP1**-R are consistent with a reversible crystalline-to-amorphous-to-crystalline transition (Fig. 8). As the cycles increase, SEM micrographs show smaller and less homogeneous crystalline material compared to the initial crystalline unground sample (Fig. S14). Similar crystalline-amorphous-crystalline transitions induced by solvatation–desolvatation processes have been recently described in $[Cu_4I_4(phosphines)]\cdot CH_3CN$ complexes.[40]

We conclude that the grinding removes CH_3CN molecules from the interior of crystalline **CP1**, significantly influencing its emission properties and causing a loss of crystallinity, but preserving the chemical composition. Subsequently, **CP1**-G is able to capture CH_3CN molecules and partially recovering its crystalline phase along with its initial photophysical properties.

The desolvation/solvation process in **CP1** is not unexpected because its crystal structure shows that CH_3CN molecules, lodged inside the voids, have weak interactions of the type C_{sp^2}-H···N≡C–Me (distances, C···N, 3.422(4) Å; H···N, 2.719(2) Å and ∡ 131.37°) with fragments of L (Fig. S6). So far, a very few Cu^{I}-halide complexes with reversible crystal-to-amorphous-to-crystal phase transformations by grinding and solvent vapors have been described, some notable examples including diimides or pyrazines as ancillary ligands.[69,85]

Mechanochromic luminescence in Cu^{I}–I complexes is commonly associated with an aggregation state change and to the increased rigidity of the systems.[69,100] However, there are scarce examples of rigidity based on reversible (de)solvatation process similar to that observed for **CP1**.

Considering forementioned outputs, the intense orange emissive of amorphous **CP1**-G can be rationalized by (1)

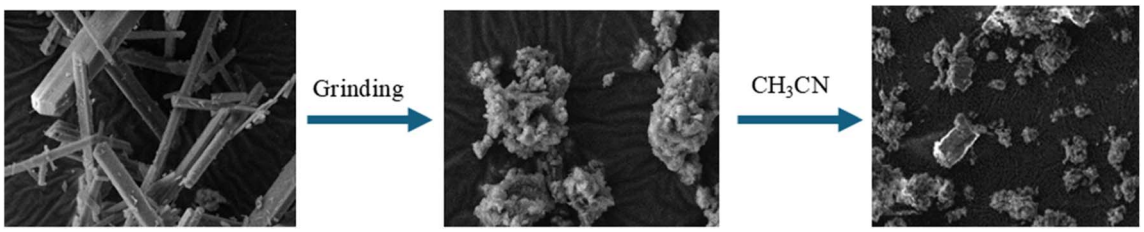

Fig. 8 SEM micrographs (1.0 μM, 5Kx) of the microcrystalline unground sample of **CP1** (left), ground sample **CP1**-G (middle) and treated sample with CH_3CN vapors, **CP1**-R (right).

elimination of inherent vibrations to solvent molecules within the **CP1** cavities, disfavoring of non-radiative pathways.[2,88,101–103] (2) compressing of the crystal packing under mechanical force which favors the cuprophilic interactions and turning on low energy color emission at 620 nm from triplet states centred transitions ^{3}CC as evidenced by the long-live lifetime in μs range.[2,3,67,71,76,94–97,104,105] Previous theoretical studies of Cu_2I_2 chains have been demonstrated contraction in $Cu^I\cdots Cu^I$ distances as far as mechanical pressure increases without modification of its structure.[3]

Interestingly, the emission spectra of **CP1** at 100 K and ground sample **CP1**-G at room temperature are similar in shape and maximum (Fig. S15), with the exception that the ground sample has a higher emission intensity.

This similarity suggests that the origin of the orange emission is the same for both samples, mainly due to cuprophilic interactions, as unambiguously demonstrated by low temperature X-ray diffraction and the higher emission intensity in **CP1**-G compared to **CP1** at 100 K may be due to the absence of CH_3CN molecules, which thereby eliminates vibrations inside emissive double-stranded Cu^I–I cluster.[43,103,104]

The vast majority of mechanochromic materials based on Cu^I-halides quench their emission under mechanical stress.[38,43,99] To our knowledge, only one green emitting mechanochromic material based on [Cu_4I_4(phosphines)] exists that turns on its emission.[41] In this context, **CP1** represents the first example of a mechanochromic compound formed by Cu^I–I with a quinoline ligand that turns on an orange emission under mechanical pressure.

2.4 Single-crystal-to-single-crystal (SCSC) transformation

An exciting topic in the modern materials coordination chemistry is the understanding of solvation phenomena in the SCSC transformation. In this line, little efforts have been invested in molecular studies focused on SCSC transformations in Cu^I–I complexes.[52,74,106]

Interestingly, heating **CP1** (~25 mg) in oven at 50 °C generated a transformation into a SCSC fashion without the need of solvents, yielding a novel non-luminescent CP with formula $^{1D}[CuI(L)]_\infty$, **CP2** (Scheme 2). Since the single crystallinity was retained during heating process, we were able to obtain the X-ray crystal structure of the solvent-free product, **CP2**, successfully.

X-ray analysis of **CP2** reveals that Cu^I atoms have an ideal trigonal planar geometry ($\Sigma\,\measuredangle$(X–Cu–X) = 360°, X = I^- or N) of [CuI_2N] type where a quinoline ring and two I^- ligands (in μ_2 environment) are coordinated (Fig. 9A). Such trigonal geometry still rare among Cu^I compounds.[107,108] The Cu–N (1.962 Å) and Cu–I (2.504(3) and 2.532(2) Å) bond lengths (Table S5) are within the range of known values. Ligand units are stacked in chains by a combination of π···π interactions and H-bonds N–H···O=C between amide groups (Table S6) similar to **CP1**. **CP2** structure grows from a zigzag 1D chain of Cu^I–I units (Fig. 9B). Conveniently for our purposes, **CP2** crystallized in the monoclinic space group $P2_1/c$ as opposed to the $C2/c$ space group of **CP1**. In this SCSC reaction, the cell volume is strongly contracted from 4734.3(3) Å to 2226.11(Å) with the release of CH_3CN molecules (Fig. 10).

All atoms in the Cu^I–I chain underwent significant changes in bond distances (Table S5). Also, intra-chain $Cu^I\cdots Cu^I$

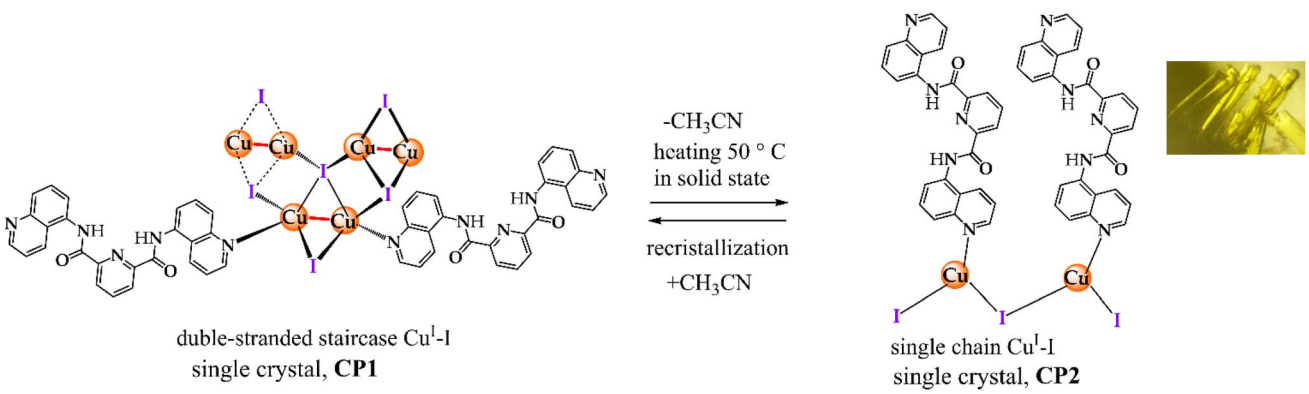

Scheme 2 Single crystal structural transformation between **CP1**–**CP2**.

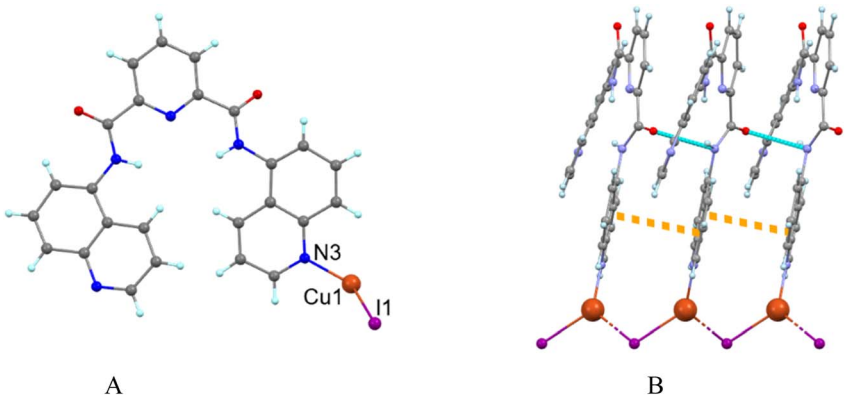

Fig. 9 (A) Perspective view of crystal structure of CP2 in a ball and stick model. (B) Single chain of CP2 formed along *c* axis showing H-bonds (N–H···O, cyan dashed lines) and π···π interactions (3.917(2) Å orange dashed lines) measured between the quinoline rings.

distances in **CP2** are longer ~36% (3.895(3) Å) compared to those found in **CP1** (2.8482(8) Å).

These long distances imply no cuprophilic interactions; hence, it can be predicted that this compound has no color emission. Indeed, **CP2** is a non-emitting species even at low temperatures or after grinding.

A comparison between the simulated PXRD pattern of **CP2** and PXRD pattern of **CP1** after heating are agreed perfectly (Fig. S16); therefore, the SCSC transformation of bulk sample seems to be taking place completely.

To verify the dynamic transformation of **CP1** to **CP2** by heating, we recorded the *in situ* PXRD pattern of **CP1** at 40 °C (Fig. S17). Interestingly, the main diffraction peaks of **CP1** and **CP2** are present, confirming thus the coexistence of the two crystalline phases.

This system is the first example of a reversible SCSC transformation that involves double-stranded staircase and zigzag chain of Cu^{I}–I described by single crystal X-ray diffraction.

Additionally, immersing crystalline **CP2** sample in CH_3CN during 10 h restores the starting PXRD pattern of **CP1** and IR-ATR spectra of **CP1** and regenerated from **CP2** in CH_3CN

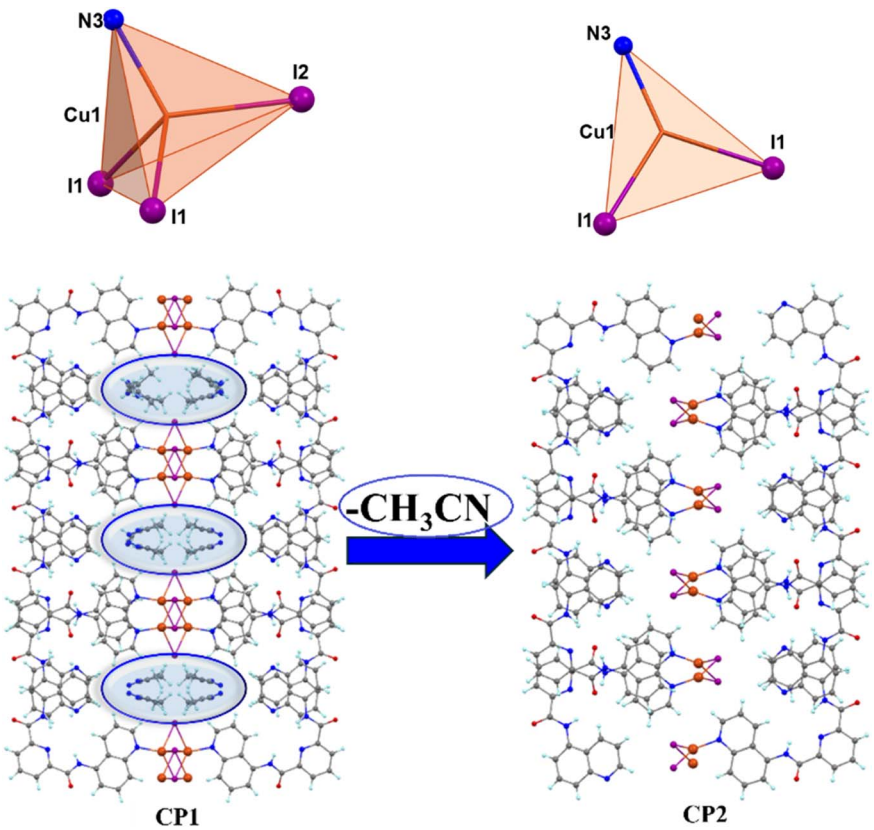

Fig. 10 Polyhedrons (top) and view along the *c* axis of a portion of crystal structures of CP1 and CP2 (bottom).

(Fig. S18) shows the signal corresponding to CH_3CN at 2250 cm^{-1}. This fact indicates a reversible structural transformation upon removal/uptake of CH_3CN from **CP2** to **CP1** by slow recrystallization.

2.5 Density functional theory (DFT) analysis

In order to gain insight related to the nature electronic transitions of **CP1**, we used DFT to optimize its geometry (Fig. S19) using X-ray data at 100 K as input file. All calculations were carried out with the Gaussian 16 suite of programs[109] at the M052X/LANL2DZ//cc-pVDZ-PP (basis set and pseudopotential for iodine) level of theory with the corresponding pseudopotentials for Cu^I (details in SI). Molecular orbitals (MOs) for **CP1** are shown in Fig. S20. At lower-energy absorptions (>287 nm), **CP1** exhibits ligand-based LUMO and HOMO based on Cu^I–I cluster, where HOMO, through HOMO-1 and HOMO-5 can be described as primarily metal centered, 3d orbitals with contribution of iodine 5p orbitals (Fig. 11). From the ground state optimized geometry, the excited state transitions for **CP1** were calculated by time-dependent density functional theory (TD-DFT) with the same model (80 excited states were requested to properly describe low energy excitations), and the outputs are compiled in Table S7 including the simulated UV-vis spectrum (Fig. S21).

In agreement with experimental UV-vis spectrum, **CP1** displays strong, high-energy peaks that have mainly ligand centered character (at 264 nm, *i.e.*, π–π*) and MLCT (285 nm and 335 nm, Fig. 11). Also, lower-energy transitions at ~479 nm are observed with oscillator value of 0.08 which are ascribed to combination of MLCT and metal cluster-centered (^{3}CC) transitions (*i.e.*, cuprophilic interactions/halide-to-metal transitions). This calculated band at 479 nm matches very to the experimentally low-intense band at 495 nm.

For the sake of comparison, the same analysis was performed on the **CP1** structure collected at 293 K, to which the same theoretical treatment as for the first structure was given and the results are collected in Table S7. No Cu^I–I orbitals were involved in the main transitions, all of which occur at high energies around 200 nm (Fig. S22 and S23) and all these transitions are of type IL.

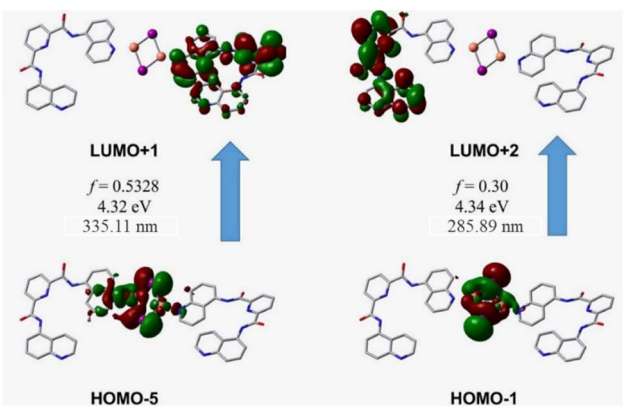

Fig. 11 Representation of selected MOs of the $[Cu_2(\mu\text{-}I)_2(L)_2]$ fragment of **CP1** with oscillator strengths (*f*) and energy levels. The input file was built using the X-ray data at 100 K, with structure optimization.

Overall, these theoretical results are consistent with temperature-dependent crystallographic studies and low-temperature lifetime measurements in microseconds. Taking together, these results provide compelling evidence that the origin of the orange emission observed in **CP1** at low temperature is due to ^{3}CC and MLCT transitions within the Cu^I–I cluster.

For comparison purposes, excited state transitions and the UV-vis plot were calculated for non-emitting complex **CP2** (Table S7 and Fig. S24). **CP2** shows two distinct high-energy bands at 182 nm and 211 nm with only a minor charge transfer contribution to the bright state at 211 nm with oscillator value of 0.08.

3 Conclusions

In summary, we have developed a new orange-emitting luminescent 1D-coordination polymer involving a double-stranded staircase Cu^I–I structure with a synthetic ditopic pyridine-2,6-bisquinoline ligand, **CP1**, and thermostability up to 220 °C.

In solid state, **CP1** exhibits reversible thermo- and mechanochromism as well as SCSC transformation whereby the 1D-double-stranded stair coordination polymer is converted into a 1D zigzag chain coordination polymer, **CP2** with marked molecular changes within the coordination environments of Cu^I and I atoms, in addition to the intra-chain $Cu^I\cdots Cu^I$ distances.

The temperature-dependent orange emission band at 612 nm has a linear behavior within the range 97–191 K, subsequently, the emission becomes very weak at room temperature. Spectroscopic and crystallographic studies at different temperatures reveal that the origin of the color emission at low temperatures hinges on mainly cuprophilic interactions that reach minimum distances of 2.8482(8) Å at 100 K. Based on multiple spectroscopic tools, PXRD and SEM-EDS, the strong increase in color emission intensity by a manual mechanical stimulus is the result of a desolvation process of CH_3CN molecules and formation of cuprophilic interactions.

Both the mechanochromism and the crystalline phase can be reversible built by exposing the amorphous material of **CP1** to CH_3CN vapors, as evidenced by SEM, PXRD, IR, quantum yield measurements in repeating cycles.

Furthermore, reversible single-crystal-to-single-crystal transformation by heating/recrystallization has been demonstrated for this Cu^I–I-bisquinoline CP with drastic molecular and crystal lattice changes.

Overall, these results highlight further the utility of a low-cost and luminescent Cu^I coordination compound in the development of multi-stimuli-responsive materials with SCSC transformation capacity.

4 Experimental section

All reagents, solvents and instrumentation are described in the SI.

4.1 Chemical synthesis of L

L was synthesized from a modification of the previously reported methodology.[110] The details of the synthesis are included in SI.

4.2 Chemical synthesis of polymer Cu^{I}–I-bisquinoline, CP1

CP1 was synthesized from the self-assembly reaction between the salt CuI (10.47 mg, 0.05 mmol) and L (20.95 mg, 0.50 mmol) in 6.0 mL of degassed CH_3CN. The reaction mixture was stirred for 1 h at room temperature, thus the yellow solid product was filtered and then washed with CH_3CN hot (yield 86.90% based on Cu). The crystallization of **CP1** was achieved by putting this compound in a 25 mL Teflon-lined stainless-steel container at 110 °C for 6 h, subsequently, slowly cooled down with a temperature ramp of 10 °C h^{-1} until room temperature. After the system cooled down, yellow single crystals with prismatic shape of **CP1** were obtained. The crystals were filtered and washed with 4 mL of CH_3CN hot. Elemental analysis (%) calcd for X-ray crystal sample $C_{25}H_{17}CuIN_5O_2$, C, 49.23; H, 2.80; N, 11.48. Found, C, 49.17; H, 2.90; N, 11.81. FT-IR (ATR) (cm^{-1}): 3347.97 ν(N–H); 3240–2957 $\nu(C–H)_{ar}$; 1978.24–1754.98 $\nu(C{=}C)_{ar}$; 1681.81 ν(C=O); 1546.27 ν(C=N). T_d (°C): 323.

4.3 Crystallographic investigations

The crystallographic data and refinement details for $\mathbf{CP1_{100K}}$, $\mathbf{CP1_{150K}}$, $\mathbf{CP1_{293K}}$ and $\mathbf{CP2_{275K}}$ are summarized in Table S1 (SI). Data for a $\mathbf{CP1_{100K}}$ and $\mathbf{CP1_{150K}}$ were collected on a Bruker APEX II CCD Diffractometer at 100 K and 150 K using Mo–Cu K_α radiation (k = 0.71073 Å) from an Incoatec ImuS sources and Helios optic monochromator.[111] Single crystals were coated with hydrocarbon oil, picked up with a nylon loop, and mounted in the cold N_2 stream of the diffractometer. Frames were collected using ω scans and integrated with SAINT.[112] Multi-scan absorption correction (SADABS) was applied.[112] The structures were solved by direct methods and refined using full-matrix least-squares on F^2 with SHELXL-2018 (ref. 113) and SHELXLE GUI.[114] The structure for $\mathbf{CP1_{100K}}$ and $\mathbf{CP1_{150K}}$ presented positional disorder in the CH_3CN solvent, which was modeled using the SIMU, RIGU and SAME instructions implemented in SHELXLE GUI.[114] For $\mathbf{CP1_{100K}}$ the proportion of all positions of solvent was refined using free variables, obtaining a total occupancy of 88.3% distributed in 4 different positions, 3 orientations in general position and one orientation in special position. The structure for $CP1_{150K}$ also presented a positional disorder in CH_3CN solvent. The occupancy was constrained to unity and distributed over four different positions using a free variable. The structure of $\mathbf{CP1_{150K}}$ was refined as a non-merohedral twin with a 60 : 40 ratio between the two domains. The hydrogens of N–H moiety were founded in the map of residual density, and their position was refined with $U_{iso} = aU_{eq}$ (where a is 1.5 for –CH_3 and –NH moieties and 1.2 for others).

Data for $\mathbf{CP1_{293}}$ and **CP2** were measured using ω scans of 0.5° per frame for 0.1 s with CuK_α radiation. The diffraction pattern was indexed, and the total number of runs and images was based on the strategy calculation from the program CrysAlisPro (Rigaku). The maximum resolution that was achieved was Θ = 79.020° (0.79 Å) for $\mathbf{CP1_{293}}$ and Θ = 68.288° (0.83 Å) for **CP2**. The total number of runs and images was based on the strategy calculation from the program CrysAlisPro (Rigaku), likewise the unit cell was refinedon 17 217 reflections.

A gaussian absorption correction was performed using CrysAlisPro 1.171.43.144a (Rigaku Oxford Diffraction, 2024) Numerical absorption correction based on gaussian integration over a multifaceted crystal model Empirical absorption correction using spherical harmonics, implemented in SCALE3 ABSPACK scaling algorithm.

The structures were solved with a space group $C2/c$ for $\mathbf{CP1_{293}}$ and $P2_1/c$ for **CP2** and determined by the ShelXT[115] structure solution program using Intrinsic Phasing and refined by Least Squares using version 2018/3 of ShelXL 2018/3.[116] All non-hydrogen atoms were refined anisotropically. Hydrogen atom positions were calculated geometrically and refined using the riding model. Special details: a solvent mask was calculated, and 154 electrons were found in a volume of 716 $Å^3$ in 1 void per unit cell. This is consistent with the presence of 1 molecule of CH_3CN per asymmetric unit which accounts for 176 electrons per unit cell.

Conflicts of interest

There are no conflicts to declare.

Data availability

CCDC 2489658 for compound **CP1** at 100 K, 2489659 at 150 K, 2489660 at 293 K and 2489661 for compound **CP2** at 275 K contain the supplementary crystallographic data for this paper.[117a–d]

Supplementary information: general information, X-ray crystallographic data, crystal packing diagrams of **CP1** and **CP2**. ^{1}H, ^{13}C, IR-ATR, MS spectra for L, **CP1**. Spectroscopic experiments, SEM-EDS micrographics and DFT calculations details. See DOI: https://doi.org/10.1039/d6ra01043a.

Acknowledgements

We thank Dr Josefina Perles Hernáez, Dr Beatriz Quiroz-García, Dr Adriana Romo Pérez, M. Sc. Elizabeth Huerta Salazar, Chem. María de la Paz Orta Pérez, M. Sc Mayra León Santiago, Dr Uvaldo Hernández Balderas, Tech. Isidoro Poveda Barriga, Tech. Luis Larumbe Canalejo, Tech. María José de la Mata Segarra, M. Sc Virginia Gómez Vidales, for technical assistance. C. P.-V. and J. J. V.-R. thank to SECIHTI to doctoral scholarship (CVU 812567 and 845962). We thank PAPIIT-UNAM IN228226 for financial support. This work was also supported by MCINN/AEI/10.13039/5011000011033 and European Union Next Generation EU/PRTR, under the National Program of Sciences and Technological Materials (PID2022-138968NB-C21, and TED2021-12941A-I00).

References

1 C. Wegeberg and O. S. Wenger, Luminescent First-Row Transition Metal Complexes, *JACS Au*, 2021, **1**, 1860–1876.
2 Y. Sagara, S. Yamane, M. Mitani, C. Weder and T. Kato, Mechanoresponsive Luminescent Molecular Assemblies: An Emerging Class of Materials, *Adv. Mater.*, 2016, **28**, 1073–1095.
3 J. Conesa-Egea, J. Gallardo-Martínez, S. Delgado, J. I. Martínez, J. Gonzalez-Platas, V. Fernández-Moreira, U. R. Rodríguez-Mendoza, P. Ocón, F. Zamora and P. Amo-Ochoa, Multistimuli Response Micro- and Nanolayers of a Coordination Polymer Based on Cu_2I_2 Chains Linked by 2-Aminopyrazine, *Small*, 2017, **13**, 1–11.
4 A. J. McConnell, C. S. Wood, P. P. Neelakandan and J. R. Nitschke, Stimuli-Responsive Metal-Ligand Assemblies, *Chem. Rev.*, 2015, **115**, 7729–7793.
5 B. Zhao, X. Gao, N. Lu and J. Deng, Color-Tunable Circularly Polarized Luminescence with Helical Polyacetylenes as Fluorescence Converters, *Adv. Opt. Mater.*, 2020, **8**, 1–8.
6 C. Wei, L. Bai, X. An, M. Xu, W. Liu, W. Zhang, M. Singh, K. Shen, Y. Han, L. Sun, J. Lin, Q. Zhao, Y. Zhang, Y. Yang, M. Yu, Y. Li, N. Sun, Y. Han, L. Xie, C. Ou, B. Sun, X. Ding, C. Xu, Z. An, R. Chen, H. Ling, W. Li, J. Wang and W. Huang, Atomic-resolved hierarchical structure of elastic π-conjugated molecular crystal for flexible organic photonics, *Chem*, 2022, **8**, 1427–1441.
7 Y. Shu, K. Ye, J. Sun, Y. Yue, C. Liu, H. Wang and R. Lu, Thermo-Induced Single-Crystal-to-Single-Crystal Transformations and Photo-Induced [2+2] Cycloaddition Reactions in Polymorphs of Chalcone-Based Molecular Crystals: Multi-Stimuli Responsive Actuators, *Chem.–A Eur. J.*, 2021, **27**, 17960–17969.
8 S. Tan, Y. Yin, W. Chen, Z. Chen, W. Tian and S. Pu, Carbazole-based highly solid-state emissive fluorene derivatives with various mechanochromic fluorescence characteristics, *Dye. Pigment.*, 2020, **177**, 108302.
9 X. Mei, K. Wei, G. Wen, Z. Liu, Z. Lin, Z. Zhou, L. Huang, E. Yang and Q. Ling, Carbazole-based diphenyl maleimides: Multi-functional smart fluorescent materials for data process and sensing for pressure, explosive and pH, *Dye. Pigment.*, 2016, **133**, 345–353.
10 Q. Zhou, M. Feng, C. Shi, M. Qian, X. Ma, R. He, X. Meng, Y. Shi, Q. Cao and L. Zheng, Multiple stimulus modulated organic crystal polymorphs with tunable luminescence behavior, *Chem. Sci.*, 2025, **16**, 9988–9997.
11 H. Yu, W. Wu, H. Zhao, K. Chen, S. Li, M. Tan, T. Wang, X. Huang, N. Wang and H. Hao, Cyanostyrene derivative with multi-stimuli responsive properties: Multicolor- and high-color-contrast switching in response to force, heat and light, *Dye. Pigment.*, 2023, **220**, 111727.
12 Y. Yao, T. Wang, H. Yu, Z. Jiang, W. Wu, H. Zhao, H. Wu, N. Wang, X. Huang and H. Hao, Organic polymorphic crystals with multi-stimuli response: excellent mechanical elasticity, novel two-stage heterotropic photochromism and self-reversible acidichromism, *Sci. China Mater.*, 2024, **67**, 2796–2806.
13 E. M. Sánchez-Carnerero, A. R. Agarrabeitia, F. Moreno, B. L. Maroto, G. Muller, M. J. Ortiz and S. De La Moya, Circularly Polarized Luminescence from Simple Organic Molecules, *Chem.–A Eur. J.*, 2015, **21**, 13488–13500.
14 H. Maeda, Y. Bando, K. Shimomura, I. Yamada, M. Naito, K. Nobusawa, H. Tsumatori and T. Kawai, Chemical-Stimuli-Controllable Circularly Polarized Luminescence from Anion-Responsive π -Conjugated Molecules, *J. Am. Chem. Soc.*, 2011, **133**, 9266–9269.
15 Y. Sawada, S. Furumi, A. Takai, M. Takeuchi, K. Noguchi and K. Tanaka, Rhodium-catalyzed enantioselective synthesis, crystal structures, and photophysical properties of helically chiral 1,1′-bitriphenylenes, *J. Am. Chem. Soc.*, 2012, **134**, 4080–4083.
16 Y. Qian, R. Zeng, Q. Jin, W. Bai, X. Zhang, R. Jian, Y. Lin and M. Yang, Multistimuli-responsive diaryldibenzofulvene derivatives and fluorescent detection of volatile organic vapors, *Dye. Pigment.*, 2024, **223**, 111979.
17 Q. F. Li, Z. Liu, L. Jin, P. Yang and Z. Wang, A water-soluble fluorescent hybrid material based on aminoclay and its bioimaging application, *RSC Adv.*, 2017, **7**, 44614–44618.
18 X. Pan, L. Lan and H. Zhang, Flexible organic crystals with multi-stimuli- responsive CPL for broadband multicolor optical waveguides, *Chem. Sci.*, 2024, **15**, 17444–17452.
19 X. Zheng, X. Liu, L. Liu, X. Li, S. Jiang, C. Niu, P. Xie, G. Liu, Z. Cao, Y. Ren, Y. Qin and J. Wang, Multi-Stimuli-Induced Mechanical Bending and Reversible Fluorescence Switching in a Single Organic Crystal, *Angew. Chem., Int. Ed.*, 2022, **61**, e202113073.
20 J. X. Wang, L. Y. Peng, Z. F. Liu, X. Zhu, L. Y. Niu, G. Cui and Q. Z. Yang, Tunable Fluorescence and Afterglow in Organic Crystals for Temperature Sensing, *J. Phys. Chem. Lett.*, 2022, **13**, 1985–1990.
21 J. Song, Y. Zhou, Z. Pan, Y. Hu, Z. He, H. Tian and X. Ma, An elastic organic crystal with multilevel stimuli-responsive room temperature phosphorescence, *Matter*, 2023, **6**, 2005–2018.
22 J. Valdes-García, J. Zamora-Moreno, C. Pinzón-Vanegas, A. O. Viviano-Posadas, D. Martínez-Otero, J. Barroso-Flores, B. Ortiz-Lopez, V. F. Ortiz-Navarrete and A. Dorazco-González, Selective Luminescent Chemosensing of Chloride Based on a Cyclometalated Platinum(II) Complex in Water: Crystal Structures, Spectroscopic Studies, Extraction, and Bioimaging, *Inorg. Chem.*, 2023, **62**, 6629–6641.
23 M. Jin and H. Ito, Solid-state luminescence of Au(I) complexes with external stimuli-responsive properties, *J. Photochem. Photobiol. C Photochem. Rev.*, 2022, **51**, 100478.
24 T. H.-Y. Chan, Z. Chen, M.-Y. Leung, M. H.-Y. Chan, E. K.-H. Wong, W. K. Tang and V. W.-W. Yam, Thermoresponsive Platinum(II) 2,6-Di(pyrid-2-yl)pyrazine Complexes with Unusual Aggregation Behavior upon Heating, *J. Am. Chem. Soc.*, 2025, **147**, 24941–24949.
25 E. V. Nykhrikova, M. A. Kiseleva, P. Kalle, S. S. Mariasina, S. A. Kozyukhin, S. V. Tatarin and S. I. Bezzubov, Stimuli-

Responsive Multifunctional Iridium(III) Complex Exhibiting Thermo-, Vapochromism, and Double Catalytic Activity, *Inorg. Chem.*, 2025, **64**, 5210–5220.

26 Y. F. Hsu, Y. C. Ho, Y. H. Liu and J. S. Yang, Dual-Phase Multi-Stimuli-Responsive Luminescence from a Pentiptycene-Linked Binuclear Cyclometalated Platinum(II) Complex, *Inorg. Chem.*, 2025, **64**, 16527–16536.

27 C. Climent, P. Alam, S. S. Pasha, G. Kaur, A. R. Choudhury, I. R. Laskar, P. Alemany and D. Casanova, Dual emission and multi-stimuli-response in iridium(III) complexes with aggregation-induced enhanced emission: Applications for quantitative CO2 detection, *J. Mater. Chem. C*, 2017, **5**, 7784–7798.

28 Y. Yang, P. Su and Y. Tang, Stimuli-Responsive Lanthanide-Based Smart Luminescent Materials for Optical Encoding and Bio-applications, *ChemNanoMat*, 2018, **4**, 1097–1120.

29 R. Jia, X. Zhou, L. Li, Y. Wang, G. Xiang, R. Pan, C. Jing and H. Gao, Multi-stimuli responsive Ln-TMA-DPA complexes with high performance temperature sensing and anti-counterfeiting applications, *Dye. Pigment.*, 2025, **240**, 112850.

30 V. Trannoy, A. N. Carneiro Neto, C. D. S. Brites, L. D. Carlos and H. Serier-Brault, Engineering of Mixed Eu^{3+}/Tb^{3+} Metal-Organic Frameworks Luminescent Thermometers with Tunable Sensitivity, *Adv. Opt. Mater.*, 2021, **9**, 1–12.

31 Q. F. Li, A. Liu, L. Fu, E. Li, D. Yue, J. T. Wang and Z. Wang, Construction of dual-mode photochromic fluorescence switching system based on water-soluble rare earth phosphates and carboxyl-containing diarylethene, *Dye. Pigment.*, 2024, **223**, 1–8.

32 B. Qin, X. Zhang, J. Dang, D. Yue, B. Zhang, W. Li, G. Gahungu, Z. Wang and J. Zhang, A 2-fold interpenetrated zinc-organic framework with Lewis basic triazole sites: luminescence sensing of Fe^{3+} and $Cr_2O_7^{2-}$, and warm white-light emission by encapsulated Ln3+ ions, *CrystEngComm*, 2022, **24**, 7058–7065.

33 K. Binnemans, P. T. Jones, B. Blanpain, T. Van Gerven and Y. Pontikes, Towards zero-waste valorisation of rare-earth-containing industrial process residues: A critical review, *J. Clean. Prod.*, 2015, **99**, 17–38.

34 A. Schlachter, F. Moutier, R. Utrera-Melero, J. Schiller, A. M. Khalil, G. Calvez, M. Scheer, K. Costuas and C. Lescop, Photoluminescent Cu(I) Assemblies with High-Temperature Solid-State Transitions as a New Class of Thermic History Tracers, *Adv. Opt. Mater.*, 2024, **12**, 1–10.

35 E. D. La Rubia, R. Garsed, F. Aguilar-Galindo, A. García-Hernán, G. Lifante-Pedrola and P. Amo-Ochoa, Low-cost, robust, and transportable devices based on Cu(I)–I cluster hybrid luminescent compounds as tetracycline sensors for contaminated waters, *J. Mater. Chem. B*, 2025, **13**, 7744–7752.

36 V. E. A. Pritchina, M. I. Rakhmanova, N. P. Gritsan, I. Y. Bagryanskaya, S. F. Malysheva and N. A. Belogorlova, Alkyl-dependent self-assembly of the first red-emitting zwitterionic $\{Cu_4I_6\}$ clusters from [alkyl-$P(2\text{-}Py)_3$]+ salts and CuI: when size matters, *Dalt. Trans.*, 2019, **48**, 2328–2337.

37 P. Dutta, A. Garai and K. Biradha, Coordination polymers containing dimeric Cu2X2 and polymeric (CuI) n clusters linked by unsymmetrical isomeric pyridine-benzimidazole linkers: modulating photophysical properties by mechanical stimuli, *RSC Mechanochem.*, 2025, **2**, 100–107.

38 J. López, M. Murillo, G. Lifante-Pedrola, E. Cantelar, J. Gonzalez-Platas, U. R. Rodríguez-Mendoza and P. Amo-Ochoa, Multi-stimulus semiconductor Cu(I)-I-pyrimidine coordination polymer with thermo- and mechanochromic sensing, *CrystEngComm*, 2022, **24**, 341–349.

39 G. Farias, C. A. M. Salla, J. Toigo, L. G. T. A. Duarte, A. J. Bortoluzzi, E. Girotto, H. Gallardo, T. D. Z. Atvars, B. de Souza and I. H. Bechtold, Enhancing the phosphorescence decay pathway of Cu(I) emitters – the role of copper–iodide moiety, *Dalt. Trans.*, 2022, **51**, 1008–1018.

40 R. Utrera-Melero, B. Huitorel, M. Cordier, J. Y. Mevellec, F. Massuyeau, C. Latouche, C. Martineau- Corcos and S. Perruchas, Combining theory and experiment to get insight into the amorphous phase of luminescent mechanochromic copper iodide clusters, *Inorg. Chem.*, 2020, **59**, 13607–13620.

41 Q. Benito, I. Maurin, T. Cheisson, G. Nocton, A. Fargues, A. Garcia, C. Martineau, T. Gacoin, J. P. Boilot and S. Perruchas, Mechanochromic luminescence of copper iodide clusters, *Chem.–A Eur. J.*, 2015, **21**, 5892–5897.

42 Y. Chen, H. X. Li, D. Liu, L. L. Liu, N. Y. Li, H. Y. Ye, Y. Zhang and J. P. Lang, Solvent effects on the assembly of $[Cu_2I_2]$- or $[Cu_4I_4]$-based coordination polymers: Isolation, structures, and luminescent properties, *Cryst. Growth Des.*, 2008, **8**, 3810–3816.

43 X. C. Shan, F. L. Jiang, L. Chen, M. Y. Wu, J. Pan, X. Y. Wan and M. C. Hong, Using cuprophilicity as a multi-responsive chromophore switching color in response to temperature, mechanical force and solvent vapors, *J. Mater. Chem. C*, 2013, **1**, 4339–4349.

44 Q. Benito, B. Baptiste, A. Polian, L. Delbes, L. Martinelli, T. Gacoin, J. P. Boilot and S. Perruchas, Pressure Control of Cuprophilic Interactions in a Luminescent Mechanochromic Copper Cluster, *Inorg. Chem.*, 2015, **54**, 9821–9825.

45 A. García-Hernán, G. Brito-Santos, E. de la Rubia, F. Aguilar-Galindo, O. Castillo, G. Lifante-Pedrola, J. Sanchiz, R. Guerrero-Lemus and P. Amo-Ochoa, Determining Factors to Understand the External Quantum Efficiency Values: Study Carried Out with Copper(I)-I and 1,2-Bis(4-pyridyl)ethane Coordination Polymers as Downshifters in Photovoltaic Modules, *Inorg. Chem.*, 2024, **63**, 4646–4656.

46 K. Tsuge, Y. Chishina, H. Hashiguchi, Y. Sasaki, M. Kato, S. Ishizaka and N. Kitamura, Luminescent copper(I) complexes with halogenido-bridged dimeric core, *Coord. Chem. Rev.*, 2016, **306**, 636–651.

47 T. Ren, H. Zhu, P. Zhu and D. Jia, Syntheses, structures, photoelectricity and photocatalysis of Cu(I) iodide hybrids and thiolate derived from dithiodipyridine, *Inorg. Chim. Acta*, 2024, **571**, 122215.

48 C. Xu, L. Lv, D. Luo and W. Liu, Synthesis, structure and photoluminescence properties of three copper(I) iodide based inorganic-organic hybrid structures with pyrazine derivatives, *New J. Chem.*, 2020, **44**, 14103–14107.

49 F. Farinella, L. Maini, P. Mazzeo, V. Fattori, F. Monti and D. Braga, White luminescence achieved by a multiple thermochromic emission in a hybrid organic-inorganic compound based on 3- picolylamine and Copper(I) Iodide., *Dalt. Trans.*, 2016, **45**, 17939–17947.

50 W. Liu, Y. Fang, G. Z. Wei, S. J. Teat, K. Xiong, Z. Hu, W. P. Lustig and J. Li, A Family of Highly Efficient CuI-Based Lighting Phosphors Prepared by a Systematic, Bottom-up Synthetic Approach, *J. Am. Chem. Soc.*, 2015, **137**, 9400–9408.

51 J. R. A. Cottam and P. J. Steel, The synthesis and crystal structures of 'necklace' 1-D coordination polymers with Cu2I2 nodes and 'extended-reach' heterocyclic bridging ligands, *Inorg. Chim. Acta*, 2014, **413**, 160–165.

52 Y. Yu, X. M. Zhang, J. P. Ma, Q. K. Liu, P. Wang and Y. Bin Dong, Cu(I)-MOF: Naked-eye colorimetric sensor for humidity and formaldehyde in single-crystal-to-single-crystal fashion, *Chem. Commun.*, 2014, **50**, 1444–1446.

53 A. Mukherjee, A. Dutta, A. D. Jana and G. K. Patra, Copper(I) and silver(I) coordination assemblies of imino-pyridyl and azino-pyridyl ligands: Syntheses, crystal structures, spectroscopic and photophysical properties, *Inorg. Chim. Acta*, 2013, **404**, 131–143.

54 S. L. Li and X. M. Zhang, Cu_3I_7 trimer and Cu_4I_8 tetramer based cuprous iodide polymorphs for efficient photocatalysis and luminescent sensing: Unveiling possible hierarchical assembly mechanism, *Inorg. Chem.*, 2014, **53**, 8376–8383.

55 L. Li, Z. Ren, X. Lü, H. Wang, Y. Chang, H. Li, B. Wu and J. Lang, Construction of $[Cu_nI_n]$-based coordination polymers via flexible benzimidazolyl-based ligands, *Sci. China Chem.*, 2010, **53**, 2083–2090.

56 L. Yao, G. Niu, J. Li, L. Gao, X. Luo, B. Xia, Y. Liu, P. Du, D. Li, C. Chen, Y. Zheng, Z. Xiao and J. Tang, Circularly Polarized Luminescence from Chiral Tetranuclear Copper(I) Iodide Clusters, *J. Phys. Chem. Lett.*, 2020, **11**, 1255–1260.

57 S. Q. Bai, K. L. Ke, D. J. Young and T. S. A. Hor, Structure and photoluminescence of cubane-like [Cu4I4] cluster-based 1D coordination polymer assembled with bis(triazole)pyridine ligand, *J. Organomet. Chem.*, 2017, **849–850**, 137–141.

58 D. Pandey, T. Samarth, V. K. Verma, C. Patel, L. Ponvijayakanthan, N. K. Jaiswal, S. Mukherjee and A. Raghuvanshi, Two-dimensional Cu(I)-MOF with mesoporous architecture towards chemiresistive NO_2 sensing, *J. Mater. Chem. A*, 2025, **13**, 11416–11424.

59 Z. Bin Wang, Y. H. Zhang, Y. L. Sun, M. H. Lv, Y. Liu, W. Z. Li, J. Luan and X. S. Zhang, Pyridine-amide-based hetero-copper iodide for the photocatalytic degradation of dyes and aerosol discolouration of VOC gases, *J. Mater. Chem. C*, 2024, **12**, 3311–3325.

60 Y. Fang, C. A. Sojdak, G. Dey, S. J. Teat, M. Li, M. Cotlet, K. Zhu, W. Liu, L. Wang, D. M. O'Carroll and J. Li, Highly efficient and very robust blue-excitable yellow phosphors built on multiple-stranded one-dimensional inorganic-organic hybrid chains, *Chem. Sci.*, 2019, **10**, 5363–5372.

61 S. Mishra, D. Pandey, K. Mishra, L. Viau and A. Raghuvanshi, Copper(I) iodide coordination polymers with triazole substituted pyridine ligands: photophysical and electrical conductivity properties, *New J. Chem.*, 2023, **47**, 19751–19759.

62 L. Jiang, Z. Wang, S. Q. Bai and T. S. A. Hor, 'click-and-click'-hybridised 1,2,3-triazoles supported Cu(I) coordination polymers for azide-alkyne cycloaddition, *Dalt. Trans.*, 2013, **42**, 9437–9443.

63 X. J. Yang, H. X. Li, Z. L. Xu, H. Y. Li, Z. G. Ren and J. P. Lang, Spacer length-controlled assembly of $[Cu_nI_n]$-based coordination polymers from CuI and bis(4-phenylpyrimidine-2-thio)alkane ligands, *CrystEngComm*, 2012, **14**, 1641–1652.

64 A. J. Blake, N. R. Brooks, N. R. Champness, P. A. Cooke, M. Crew, A. M. Deveson, L. R. Hanton, P. Hubberstey, D. Fenske and M. Schröder, Copper(I) iodide coordination networks–controlling the placement of $(CuI)_\infty$ ladders and chains within two-dimensional sheets, *Cryst. Eng.*, 1999, **2**, 181–195.

65 J. Vallejos, I. Brito, A. Cárdenas, M. Bolte, J. Llanos and M. López-Rodríguez, A novel double-stranded staircase Cu(I)-iodide coordination polymer based on bis(4-pyridyl-carboxylate) ligand with flexible propyl spacer: Syntheses, crystal structure, luminescence properties and thermal stability, *Inorg. Chem. Commun.*, 2012, **24**, 59–62.

66 D. Malpicci, D. Blasi, D. Marinotto, A. Forni, E. Cariati, E. Lucenti and L. Carlucci, A Rare Structural Motif for a Luminescent Cu(I) Coordination Polymer with 3-(Pyridin-2-yl)triimidazotriazine, *Crystals*, 2023, **13**, 19.

67 N. M. Khatri, M. H. Pablico-Lansigan, W. L. Boncher, J. E. Mertzman, A. C. Labatete, L. M. Grande, D. Wunder, M. J. Prushan, W. Zhang, P. S. Halasyamani, J. H. S. K. Monteiro, A. De Bettencourt-Dias and S. L. Stoll, Luminescence and Nonlinear Optical Properties in Copper(I) Halide Extended Networks, *Inorg. Chem.*, 2016, **55**, 11408–11417.

68 J. Pospisil, I. Jess, C. Näther, M. Necas and P. Taborsky, Luminescence properties of 'double-stranded staircase' copper(I) halide coordination polymers with N-containing ligands, *New J. Chem.*, 2011, **35**, 861–864.

69 M. Murillo, J. Álvarez-Conde, R. Wannemacher, J. Cabanillas-González, J. González-Platas, U. R. Rodríguez-Mendoza, A. Liang, R. Turnbull, D. Errandonea, J. I. Martínez and P. Amo-Ochoa, A 1D Cu(I)-I-pyrazine coordination polymer with controlled pressure-induced phase transition and opto-electronic response depending on mechanical stimuli, temperature, and CuI content, *J. Mater. Chem. C*, 2022, **10**, 18004–18016.

70 Z. F. Wu, C. Wang, X. Liu, K. Tan, Z. Fu, S. J. Teat, Z. W. Li, X. Hei, X. Y. Huang, G. Xu and J. Li, Confinement of 1D Chain and 2D Layered CuI Modules in K-INA-R

Frameworks via Coordination Assembly: Structure Regulation and Semiconductivity Tuning, *J. Am. Chem. Soc.*, 2023, **145**, 19293–19302.

71 A. Schlachter and P. D. Harvey, Properties and applications of copper halide-chalcogenoether and -chalcogenone networks and functional materials, *J. Mater. Chem. C*, 2021, **9**, 6648–6685.

72 N. V. S. Harisomayajula, S. Makovetskyi and Y. C. Tsai, Cuprophilic interactions in and between Molecular Entities, *Chem.–A Eur. J.*, 2019, **25**, 8936–8954.

73 J. Conesa-Egea, F. Zamora and P. Amo-Ochoa, Perspectives of the smart Cu-Iodine coordination polymers: A portage to the world of new nanomaterials and composites, *Coord. Chem. Rev.*, 2019, **381**, 65–78.

74 T. H. Kim, Y. W. Shin, J. H. Jung, J. S. Kim and J. Kim, Crystal-to-crystal transformation between three CuI coordination polymers and structural evidence for luminescence thermochromism, *Angew. Chem., Int. Ed.*, 2008, **47**, 685–688.

75 X. Hei and J. Li, All-in-one: a new approach toward robust and solution-processable copper halide hybrid semiconductors by integrating covalent, coordinate and ionic bonds in their structures, *Chem. Sci.*, 2021, **12**, 3805–3817.

76 A. Aguirrechu-Comerón, R. Hernández-Molina, P. Rodríguez-Hernández, A. Muñoz, U. R. Rodríguez-Mendoza, V. Lavín, R. J. Angel and J. Gonzalez-Platas, Experimental and ab initio study of catena(bis(μ2-iodo)-6-methylquinoline-copper(I)) under pressure: synthesis, crystal structure, electronic, and luminescence properties, *Inorg. Chem.*, 2016, **55**, 7476–7484.

77 A. Dorazco-González, M. F. Alamo, C. Godoy-Alcántar, H. Höpfl and A. K. Yatsimirsky, Fluorescent anion sensing by bisquinolinium pyridine-2,6-dicarboxamide receptors in water, *RSC Adv.*, 2014, **4**, 455.

78 Y. Song, R. Q. Fan, H. J. Zhang, Z. W. Liu, X. T. Wang, C. T. Tan, Y. L. Yang and Y. L. Wang, Luminescent properties of Ag(I)/Cu(I) coordination polymers: Crystal structures and high intensity luminescence of a PMMA-doped hybrid material based on a quinoline-2,3-dicarboxylic acid ligand, *RSC Adv.*, 2015, **5**, 17343–17353.

79 E. Lee, H. Ju, J. H. Jung, M. Ikeda, Y. Habata and S. S. Lee, Conventional and Mechanochemical Syntheses of Copper(I) Iodide Luminescent MOF with Bis(amidoquinoline) and Its Application for the Detection of Amino Acid in Aqueous Solution, *Inorg. Chem.*, 2019, **58**, 1177–1183.

80 A. O. Viviano-Posadas, U. Romero-Mendoza, I. J. Bazany-Rodríguez, R. V. Velázquez-Castillo, D. Martínez-Otero, J. M. Bautista-Renedo, N. González-Rivas, R. Galindo-Murillo, M. K. Salomón-Flores and A. Dorazco-González, Efficient fluorescent recognition of ATP/GTP by a water-soluble bisquinolinium pyridine-2,6-dicarboxamide compound. Crystal structures, spectroscopic studies and interaction mode with DNA, *RSC Adv.*, 2022, **12**, 27826–27838.

81 J. Valdes-García, J. Zamora-Moreno, M. K. Salomón-Flores, D. Martínez-Otero, J. Barroso-Flores, A. K. Yatsimirsky, I. J. Bazany-Rodríguez and A. Dorazco-González, Fluorescence Sensing of Monosaccharides by Bis-boronic Acids Derived from Quinolinium Dicarboxamides: Structural and Spectroscopic Studies, *J. Org. Chem.*, 2023, **88**, 2174–2189.

82 A. L. Spek, PLATON SQUEEZE: A tool for the calculation of the disordered solvent contribution to the calculated structure factors, *Acta Crystallogr. Sect. C Struct. Chem.*, 2015, **71**, 9–18.

83 L. D. Rosales-Vázquez, V. Sánchez-Mendieta, A. Dorazco-González, D. Martínez-Otero, I. García-Orozco, R. A. Morales-Luckie, J. Jaramillo-Garcia and A. Téllez-López, Cadmium-1,4-cyclohexanedicarboxylato coordination polymers bearing different di-alkyl-2,2'-bipyridines: Syntheses, crystal structures and photoluminescence studies, *Dalt. Trans.*, 2017, **46**, 12516–12526.

84 M. S. Deshmukh, A. Yadav, R. Pant and R. Boomishankar, Thermochromic and mechanochromic luminescence umpolung in isostructural metal-organic frameworks based on Cu_6I_6 clusters, *Inorg. Chem.*, 2015, **54**, 1337–1345.

85 G. Kang, Y. Jeon, K. Y. Lee, J. Kim and T. H. Kim, Reversible Luminescence Vapochromism and Crystal-to-Amorphous-to-Crystal Transformations of Pseudopolymorphic Cu(I) Coordination Polymers, *Cryst. Growth Des.*, 2015, **15**, 5183–5187.

86 A. Kobayashi, R. Arata, T. Ogawa, M. Yoshida and M. Kato, Effect of Water Coordination on Luminescent Properties of Pyrazine-Bridged Dinuclear Cu(I) Complexes, *Inorg. Chem.*, 2017, **56**, 4280–4288.

87 Y. Thefioux, M. Cordier, F. Massuyeau, C. Latouche, C. Martineau-Corcos and S. Perruchas, Polymorphic Copper Iodide Anions: Luminescence Thermochromism and Mechanochromism of $(PPh_4)_2[Cu_2I_4]$, *Inorg. Chem.*, 2020, **59**, 5768–5780.

88 J. Conesa-Egea, N. Nogal, J. I. Martínez, V. Fernández-Moreira, U. R. Rodríguez-Mendoza, J. González-Platas, C. J. Gómez-García, S. Delgado, F. Zamora and P. Amo-Ochoa, Smart composite films of nanometric thickness based on copper-iodine coordination polymers. Toward sensors, *Chem. Sci.*, 2018, **9**, 8000–8010.

89 S. Perruchas, X. F. L. Goff, S. Maron, I. Maurin, F. Guillen, A. Garcia, T. Gacoin and J. P. Boilot, Mechanochromic and thermochromic luminescence of a copper iodide cluster, *J. Am. Chem. Soc.*, 2010, **132**, 10967–10969.

90 B. Wang, Y. Fu, Y. Shen, P. Wang, Y. Chen, F. Feng, Z. Xu, W. Huang and D. Wu, Suppressing the Thermal Quenching Effect via a Cluster Conformer in Copper(I)-Iodide Coordination Polymeric Phosphors for High-Power White LED Lighting, *Inorg. Chem.*, 2024, **63**, 8070–8078.

91 Q. Han, X. Ye, X. Zheng, Q. Guo, Q. Lin, C. Li, J. Jiang, Y. Liu and X. Tao, Multiple stimuli triggered structural isomerization of copper iodide-pyridine crystals, *CrystEngComm*, 2022, **24**, 788–795.

92 S. Perruchas, Molecular copper iodide clusters: a distinguishing family of mechanochromic luminescent compounds, *Dalt. Trans.*, 2021, **50**, 12031–12044.
93 I. De, D. Rennes and R. Cedex, Bonding in Tetrahedral Cu4(μ_3-X)$_4$L$_4$ Copper (I) Clusters : A DFT, *Inorg. Chem.*, 2004, **43**, 4012–4018.
94 L. Si, Q. Fu, Z. Shi, T. Zhang, Q. Hou, Z. Xu and S. Ai, The fluorescent detection of biothiols and antimicrobial study based on copper(I) iodide coordination polymer, *Dye. Pigment.*, 2023, **215**, 111228.
95 E. Cariati, E. Lucenti, C. Botta, U. Giovanella, D. Marinotto and S. Righetto, Cu(I) hybrid inorganic-organic materials with intriguing stimuli responsive and optoelectronic properties, *Coord. Chem. Rev.*, 2016, **306**, 566–614.
96 M. Jin, R. Ando and H. Ito, Distinct Fold-Mode Formation of Crystalline Cu(I) Helical Coordination Polymers with Alternation of the Solid-State Emission Using Shape of the Counter Anions, *Inorg. Chem.*, 2022, **61**, 3–9.
97 M. El Sayed Moussa, A. M. Khalil, S. Evariste, H. L. Wong, V. Delmas, B. Le Guennic, G. Calvez, K. Costuas, V. W. W. Yam and C. Lescop, Intramolecular rearrangements guided by adaptive coordination-driven reactions toward highly luminescent polynuclear Cu(I) assemblies, *Inorg. Chem. Front.*, 2020, **7**, 1334–1344.
98 S. Perruchas, C. Tard, X. F. Le Goff, A. Fargues, A. Garcia, S. Kahlal, J. Y. Saillard, T. Gacoin and J. P. Boilot, Thermochromic luminescence of copper iodide clusters: The case of phosphine ligands, *Inorg. Chem.*, 2011, **50**, 10682–10692.
99 X. Zhang, Z. Chi, Y. Zhang, S. Liu and J. Xu, Recent advances in mechanochromic luminescent metal complexes, *J. Mater. Chem. C*, 2013, **1**, 3376–3390.
100 E. Kwon, J. Kim, K. Y. Lee and T. H. Kim, Non-phase-transition luminescence mechanochromism of a copper(I) coordination polymer, *Inorg. Chem.*, 2017, **56**, 943–949.
101 L. li Deng, X. long Huang, S. mao Liu, Y. ping Yang, H. feng He, L. Fu, H. yun Chen, F. Zhao, H. ying Xia and Z. hua Xiong, AIE-active N-heterocyclic carbene Cu(I) complexes: Stimuli-responsive with hypsochromic or bathochromic mechanochromic phosphorescence through switchable C–H$\cdots$F interactions, *Dye. Pigment.*, 2024, **230**, 112346.
102 R. Czerwieniec, M. J. Leitl, H. H. H. Homeier and H. Yersin, Cu(I) complexes – Thermally activated delayed fluorescence. Photophysical approach and material design, *Coord. Chem. Rev.*, 2016, **325**, 2–28.
103 H. Park, E. Kwon, H. Chiang, H. Im, K. Y. Lee, J. Kim and T. H. Kim, Reversible Crystal Transformations and Luminescence Vapochromism by Fast Guest Exchange in Cu(I) Coordination Polymers, *Inorg. Chem.*, 2017, **56**, 8287–8294.
104 Q. Benito, X. F. Le Goff, S. Maron, A. Fargues, A. Garcia, C. Martineau, F. Taulelle, S. Kahlal, T. Gacoin, J. P. Boilot and S. Perruchas, Polymorphic copper iodide clusters: Insights into the mechanochromic luminescence properties, *J. Am. Chem. Soc.*, 2014, **136**, 11311–11320.
105 J. Troyano, J. Perles, P. Amo-Ochoa, J. I. Martínez, M. Concepción Gimeno, V. Fernández-Moreira, F. Zamora and S. Delgado, Luminescent Thermochromism of 2D Coordination Polymers Based on Copper(I) Halides with 4-Hydroxythiophenol, *Chem. –A Eur. J.*, 2016, **22**, 18027–18035.
106 Y. L. Jai, Y. L. So, W. Sim, K. M. Park, J. Kim and S. L. Shim, Temperature-dependent 3-D CuI coordination polymers of calix[4]-bis- dithiacrown: Crystal-to-crystal transformation and photoluminescence change on coordinated solvent removal, *J. Am. Chem. Soc.*, 2008, **130**, 6902–6903.
107 T. C. Wu, F. Z. Zhao, Q. L. Hu, Y. S. Cui, T. H. Huang, D. Zheng, Q. Liu, Y. Lei, L. Jia and C. Luo, Structural characterization, DFT studied, luminescent properties of cationic/neutral three-coordinated copper(I) complexes and application in warm-white light-emitting diode, *Appl. Organomet. Chem.*, 2020, **34**, 1–10.
108 J. Föller, M. Kleinschmidt and C. M. Marian, Phosphorescence or Thermally Activated Delayed Fluorescence? Intersystem Crossing and Radiative Rate Constants of a Three- Coordinate Copper(I) Complex Determined by Quantum-Chemical Methods, *Inorg. Chem.*, 2016, **55**, 7508–7516.
109 M. J. Frisch, G. W. Trucks, H. B. Schlegel, G. E. Scuseria, M. A. Robb, J. R. Cheeseman, G. Scalmani, V. Barone, G. A. Petersson, H. Nakatsuji, X. Li, M. Caricato, A. V Marenich, J. Bloino, B. G. Janesko, R. Gomperts, B. Mennucci, H. P. Hratchian, J. V Ortiz, A. F. Izmaylov, J. L. Sonnenberg, D. Williams-Young, F. Ding, F. Lipparini, F. Egidi, J. Goings, B. Peng, A. Petrone, T. Henderson, D. Ranasinghe, V. G. Zakrzewski, J. Gao, N. Rega, G. Zheng, W. Liang, M. Hada, M. Ehara, K. Toyota, R. Fukuda, J. Hasegawa, M. Ishida, T. Nakajima, Y. Honda, O. Kitao, H. Nakai, T. Vreven, K. Throssell, J. A. Montgomery Jr., J. E. Peralta, F. Ogliaro, M. J. Bearpark, J. J. Heyd, E. N. Brothers, K. N. Kudin, V. N. Staroverov, T. A. Keith, R. Kobayashi, J. Normand, K. Raghavachari, A. P. Rendell, J. C. Burant, S. S. Iyengar, J. Tomasi, M. Cossi, J. M. Millam, M. Klene, C. Adamo, R. Cammi, J. W. Ochterski, R. L. Martin, K. Morokuma, O. Farkas, J. B. Foresman and D. J. Fox, *Gaussian 16 Revision C01*, Gaussian, Inc., 2016, Wallingford CT, 16.
110 J. Zamora-Moreno, M. K. Salomón-Flores, J. Valdes-García, C. Pinzón-Vanegas, D. Martínez-Otero, J. Barroso-Flores, R. Villamil-Ramos, M. I. Romero-Solano and A. Dorazco-González, Water-soluble fluorescent chemosensor for sorbitol based on a dicationic diboronic receptor. Crystal structure and spectroscopic studies, *RSC Adv.*, 2023, **13**, 32185–32198.
111 *APEX 2 Software Suite*, Bruker AXS Inc., Madison, Wisconsin, USA.
112 *B. A. Inc.*, Bruker SAINT and SADABS, Madison, Wisconsin, USA, 2007.
113 G. M. Sheldrick, A short history of SHELX, *Acta Crystallogr. Sect. A Found. Crystallogr.*, 2007, **64**, 112–122.

114 C. B. Hübschle, G. M. Sheldrick and B. Dittrich, ShelXle: A Qt graphical user interface for SHELXL, *J. Appl. Crystallogr.*, 2011, **44**, 1281–1284.
115 G. M. Sheldrick, SHELXT - Integrated space-group and crystal-structure determination, *Acta Crystallogr. Sect. A Found. Crystallogr.*, 2015, **71**, 3–8.
116 G. M. Sheldrick, Crystal structure refinement with SHELXL, *Acta Crystallogr. Sect. C Struct. Chem.*, 2015, **71**, 3–8.
117 (*a*) CCDC 2489658: Experimental Crystal Structure Determination, 2026, DOI: 10.5517/ccdc.csd.cc2pkpkj; (*b*) CCDC 2489659: Experimental Crystal Structure Determination, 2026, DOI: 10.5517/ccdc.csd.cc2pkplk; (*c*) CCDC 2489660: Experimental Crystal Structure Determination, 2026, DOI: 10.5517/ccdc.csd.cc2pkpml; (*d*) CCDC 2489661: Experimental Crystal Structure Determination, 2026, DOI: 10.5517/ccdc.csd.cc2pkpnm.